

NEW APPROACHES IN SCIENCE AND ENGINEERING

Editor:

Assoc. Prof. Dr. Gökhan ÇAYLI

ARTİKEL AKADEMİ: 329

New Approaches in Science and Engineering

Editor: Assoc. Prof. Dr. Gökhan ÇAYLI
Istanbul University-Cerrahpaşa
Department of Engineering Sciences
Orcid No: 0000-0002-3395-5642

ISBN 978-625-6627-68-0

1st Edition: December 2024

Publisher Certificate No: 19708

Cover and Book Design: Artikel Akademi

PRINTING: Uzunist Dijital Matbaa Anonim Şirketi
Akçaburgaz Mah.1584.Sk.No:21 / Esenyurt - İSTANBUL

Certification No.: 68922

©Karadeniz Kitap - 2024

Except for quotations to be made in accordance with academic ethical rules and short quotations to be made for promotional purposes, printing, publication, copying, reproduction or distribution, in whole or in part, by electronic, mechanical or photocopying, cannot be made without written permission.

KARADENİZ KİTAP LTD. ŞTİ.
Koşuyolu Mah. Mehmet Akfan Sok. No:67/3 Kadıköy-İstanbul
Tel: 0 216 428 06 54 // 0530 076 94 90

mail: destek@artikelakademi.com
www.artikelakademi.com

NEW APPROACHES IN SCIENCE AND ENGINEERING

Editor:

Assoc. Prof. Dr. Gökhan ÇAYLI

WRITERS

Prof. Dr. Aysen E. OZEL

Prof. Dr. Aysel ERSOY

Prof. Dr. Sefa CELIK

Assist. Prof. Dr. Abdurrahim AKGÜNDOĞDU

Assoc.Prof. Dr. Alev ER

Assoc. Prof. Cengiz Polat UZUNOĞLU

Assoc. Prof. Dr. Gökhan ÇAYLI

Res. Asst. Dr. Fatih ATALAR

Dr. Emin ÖZDEMİR

Başak AKİPEK

Serap ÇEKLİ

CONTENTS

INTRODUCTION.....7

CHAPTER 1

NOISE REMOVAL IN ECG SIGNALS: A DEEP LEARNING-BASED
APPROACH.....9
Abdurrahim AKGÜNDOĞDU

CHAPTER 2

MOLECULAR DOCKING STUDIES OF ANTIDIABETIC
COMPOUNDS WITH DPPIV PROTEASE.....23
Alev ER & Sefa CELIK

CHAPTER 3

THEORETICAL FRAMEWORK FOR MOLECULAR DOCKING OF SOTORASIB
AND REPOTRECTINIB WITH EGFR RECEPTORS33
Sefa CELIK & Aysen E. OZEL

CHAPTER 4

BUSHING TYPES OF POWER TRANSFORMERS43
Başak AKİPEK & Cengiz Polat UZUNOĞLU & Serap ÇEKLİ

CHAPTER 5

MEASUREMENT OF INSULATION PERFORMANCE OF TRANSFORMER
DIELECTRIC LIQUIDS BY HARMONIC CURRENT ANALYSIS.....59
Fatih ATALAR & Aysel ERSOY

CHAPTER 6

BIO-BASED POLYURETHANES.....73

Gökhan ÇAYLI & Emin ÖZDEMİR

CHAPTER 7

BIOBASED ANTIBACTERIAL MATERIALS.....85

Gökhan ÇAYLI

CHAPTER 8

MOLECULAR DOCKING STUDIES OF CEPHALOSPORIN AND
OXYTETRACYCLINE WITH ESCHERICHIA COLI DNA GYRASE.....95

Alev ER & Sefa CELİK & Aysen E. OZEL & Sevim AKYUZ

PREFACE

The examples presented in this book are from the work of scientists doing research in a wide variety of disciplines. Within the scientific fields of physics, chemistry, and electrical electronics, the book provides examples of investigations that have been conducted. Molecular docking studies, power transformers, noise reduction in electrocardiogram (ECG) data, and examination of the insulation properties of dielectric transformer fluids are some of the subjects that are discussed in this book. Furthermore, biobased polyurethanes and biobased antimicrobial compounds are also included. In the past, each scientific field was distinguished from the others by definite borders, which resulted in the separation of these branches into more specialized sub-branches and the conduct of investigations within this area of study. On the other hand, the creation of new views and the rise of multidisciplinary studies in the fields of science and engineering have been brought about as a result of the progression of technology and the emergence of more complex current demands. I am positive that this book will serve as a source of motivation for this field.

I am grateful to all of my coworkers who contributed to the publication of the book.

December-2024
Assoc. Prof. Gökhan ÇAYLI
Istanbul University-Cerrahpaşa,
Faculty of Engineering, Department of Engineering Sciences

CHAPTER 1

NOISE REMOVAL IN ECG SIGNALS: A DEEP LEARNING-BASED APPROACH

Assist. Prof. Dr. Abdurrahim AKGÜNDOĞDU

Istanbul University-Cerrahpaşa,

Department of Electrical and Electronics Engineering

ORCID: 0000-0001-8113-0277

1. INTRODUCTION

Electrocardiography (ECG) is a critical medical imaging technique that records the electrical signals of cardiac activity. It provides invaluable insights into heart function and plays a pivotal role in diagnosing and monitoring cardiovascular diseases (Castells et al., 2007). The precision of ECG measurements is paramount in clinical diagnostics, as even minor signal distortions can lead to misinterpretation of cardiac conditions and potentially compromise patient care.

ECG signals are inherently susceptible to various types of noise that can significantly compromise their diagnostic value. These noise sources are diverse and complex, originating from physiological interference, instrumental noise, and environmental factors. Physiological interferences include muscle tremors, respiration artifacts, electrode motion, and baseline wander caused by patient movements or breathing. Instrumental noise stems from medical devices and recording equipment, introducing electromagnetic interference, power line noise (50/60 Hz), and electronic circuit imperfections. Environmental factors such as external electromagnetic fields and ambient electronic noise further contribute to signal degradation.

Traditionally, noise reduction techniques have relied on conventional filter-based methods, such as low-pass, high-pass, and band-pass filters (Zhang et al., 2010; Sayadi & Shamsollahi, 2008). However, these approaches present significant limitations in adapting to complex, multi-source noise environments. They often result in signal distortion, loss of critical diagnostic information, and reduced effectiveness when handling non-stationary noise characteristics. Multi-channel processing techniques have emerged as an alternative approach, offering more sophisticated noise reduction strategies, but these methods typically require complex computational architectures, substantial processing power, and intricate signal alignment techniques (Fotiadou & Vullings, 2020; Sameni et al., 2006).

The advent of deep learning technologies has revolutionized medical signal processing, offering unprecedented capabilities in pattern recognition, feature extraction, and noise elimination. Deep learning models, particularly neural network architectures like denoising autoencoders (DAEs), demonstrate remarkable potential in addressing the complex challenges of ECG signal noise removal (Arsene et al., 2019; Antczak, 2018). Denoising autoencoders represent a sophisticated approach to signal reconstruction, capable of learning low-dimensional representations of clean signals, identifying and isolating noise patterns, and reconstructing high-fidelity signals by effectively separating meaningful cardiac electrical information from interference.

This study introduces an innovative deep learning-based denoising autoencoder model specifically designed for ECG signal noise removal. The proposed approach is distinguished by its comprehensive training using both real and synthetically generated noisy ECG signals, rigorous performance evaluation, and comparative analysis against traditional noise reduction techniques. The model was meticulously evaluated using a comprehensive set of performance metrics, including Mean Squared Error (MSE), Mean Absolute Error (MAE), R^2 Score, Structural Similarity Index (SSIM), and Signal-to-Noise Ratio (SNR).

Experimental results demonstrate the model's superior noise removal capabilities, showcasing significant improvements in signal quality and diagnostic reliability compared to conventional methodological approaches. By addressing the critical challenge of ECG signal noise removal, this research contributes to advancing medical signal processing technologies, potentially enhancing diagnostic accuracy and supporting more reliable cardiovascular disease detection and monitoring.

2. MATERIAL AND METHODS

2.1. Data Processing and Model Training

The data processing and model training process comprised the steps summarized in Figure 1. First, data obtained from the MIT-BIH Database were processed by adding artificial noise. Subsequently, the data were segmented and divided into 70% training and 30% testing datasets. A denoising autoencoder architecture was employed for noise reduction, and the model was trained over 1000 epochs. After training, the model's performance was evaluated using validation and test datasets, with results reported based on metrics such as MSE, MAE, R^2 score, Pearson correlation, SSIM, and SNR.

2.2. Data Preprocessing

The ECG data used in this study were obtained from the MIT-BIH Arrhythmia Database, a widely used resource in the diagnosis of cardiovascular diseases that contains 48-hour ECG recordings with various arrhythmic events (Moody & Mark, 2001). During data processing, each ECG recording was divided into 500-sample segments, enabling analysis of shorter time intervals, which better capture signal behaviors. These segments were mixed with artificial noise to create noisy ECG signals, ensuring the model can handle real-world noisy signals. Artificial noise was generated using white noise or random data with Gaussian distribution.

Finally, all data were divided into three main sets for training, validation, and testing. The training set enabled the model to learn, the validation set helped tune hyperparameters, and the test set evaluated overall model performance. The data were split as 70% training, 15% validation, and 15% testing.

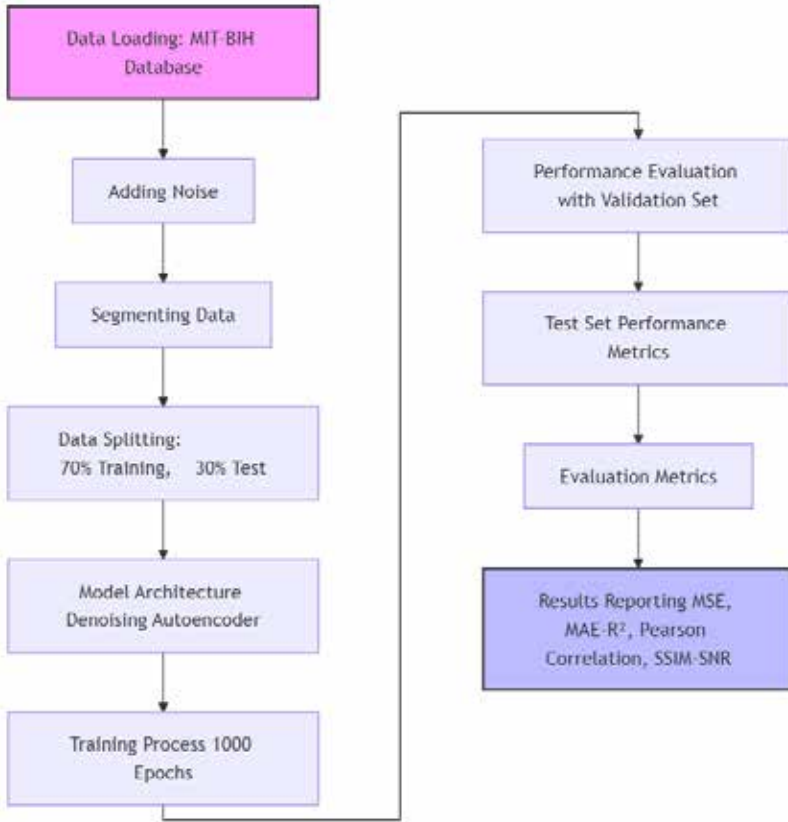


Figure 1. Workflow Diagram: Steps of data processing and model training.

2.3. Denoising Autoencoder Model

This study employed a deep learning-based denoising autoencoder model as its core. Autoencoders are artificial neural networks based on an encoder-decoder architecture, commonly used for data compression and dimensionality reduction (Vincent et al., 2008). The model’s primary goal is to reconstruct the original signal from a noisy input signal.

Encoder Network:

The encoder takes the input signal and transforms it into a lower-dimensional latent representation, extracting key features from noisy signals. Mathematically, the encoder function can be expressed as:

$$h = f(E(x)) = f(w_{enc} \cdot x + b_{enc}) \quad 1$$

where x is the noisy input signal, w_{enc} represents encoder weights, b_{enc} denotes bias terms, and h is the lower-dimensional representation (Vincent et al., 2010).

Decoder Network:

The decoder reconstructs the original signal from the lower-dimensional representation. It consists of layers that progressively increase the representation's dimensionality. The loss function used in this process is typically the Mean Squared Error (MSE), which minimizes the difference between the predicted and true signals. Mathematically, the decoder function is expressed as:

$$x' = g(D(h)) = g(w_{dec} \cdot h + b_{dec}) \quad 2$$

where x' represents the reconstructed signal, w_{dec} denotes decoder weights, and b_{dec} refers to bias terms (Vincent et al., 2010).

2.3.1. Model Training and Evaluation

The model was trained using the Mean Squared Error loss function. MSE calculates the average of the squared differences between the predicted and actual signals, serving as a common measure of error magnitude (Chai & Draxler, 2014). MSE loss is defined as:

$$MSE = \frac{1}{N} \sum_{i=1}^N (x_i - x'_i)^2 \quad 3$$

where N represents the number of samples in the signal, x_i the original signal, and x'_i the model's predicted denoised signal.

During training, this loss function was minimized using backpropagation. The optimization process employed algorithms such as Adam or Stochastic Gradient Descent (SGD) (Kingma, 2014). By squaring the errors, MSE penalizes larger discrepancies more heavily, making it suitable for achieving higher accuracy.

Hyperparameter Configuration:

The performance of the proposed denoising autoencoder heavily depends

on its carefully tuned hyperparameters. These parameters control the structure and optimization process of the model, ensuring efficient learning and accurate denoising of ECG signals. These hyperparameters were chosen based on prior experiments and literature, ensuring a balance between computational efficiency and performance. Table 1 provides the full set of parameters.

Table 1. Hyperparameters for denoising autoencoder model.

Hyperparameter	Value
Input Dimension	500
Encoder Layers	256 (ReLU) → 128 (ReLU)
Decoder Layers	256 (ReLU) → 500 (Tanh)
Dropout	10%
Batch Size	32
Epochs	1000
Loss Function	Mean Squared Error
Optimizer	Adam
Learning Rate	0.001
Train/Test Split	70% Train, 30% Test
Validation Split	15% of Training Data

To evaluate model performance, several quantitative metrics were employed. These metrics are widely used to measure accuracy, predictive power, and noise removal efficacy. Below are detailed explanations and formulae for each metric used.

2.3.2. Mean Absolute Error (MAE)

Mean Absolute Error (MAE) computes the mean of the absolute differences between predicted and actual values. Unlike MSE, MAE is less sensitive to outliers. It is calculated as:

$$MAE = \frac{1}{N} \sum_{i=1}^n |y_i - \hat{y}_i| \quad 4$$

where y_i represents the actual values and \hat{y}_i the predicted values (Chai & Draxler, 2014). MAE provides a robust measure of average error magnitude.

2.3.3. Coefficient of Determination (R^2 Score)

The R^2 score measures the explanatory power of the model, quantifying how well the predictions align with actual data. It is defined as:

$$R^2 = 1 - \frac{\sum_{i=1}^n (y_i - \hat{y}_i)^2}{\sum_{i=1}^n (y_i - \bar{y})^2} \quad 5$$

where \bar{y} is the mean of the actual values. An R^2 score of 1 indicates perfect predictions, while 0 signifies no explanatory power (Ruppert, 2004).

2.3.4. Pearson Correlation Coefficient (R)

Pearson's correlation coefficient evaluates the linear relationship between predicted and actual values. Its range is between -1 and 1, where values close to 1 indicate a strong positive correlation. The formula is:

$$R = \frac{\sum_{i=1}^n (y_i - \hat{y}_i)(\hat{y}_i - \bar{\hat{y}})}{\sqrt{\sum_{i=1}^n (y_i - \hat{y}_i)^2} \sqrt{\sum_{i=1}^n (\hat{y}_i - \bar{\hat{y}})^2}} \quad 6$$

where $\bar{\hat{y}}$ is the mean of the predicted values. A high R value indicates that the model's predictions are close to reality.

2.3.5. Structural Similarity Index (SSIM)

The Structural Similarity Index measures the perceived quality and similarity between two signals, considering luminance, contrast, and structural features (Bakurov et al., 2022). While SSIM is commonly applied to images, it can also be adapted for time-series data. It is defined as:

$$SSIM(x, y) = \frac{(2\mu_x\mu_y + c_1)(2\sigma_{xy} + c_2)}{(\mu_x^2 + \mu_y^2 + c_1)(\sigma_x^2 + \sigma_y^2 + c_2)} \quad 7$$

where μ_x , μ_y and, σ_x , σ_y represent the mean and variance of the signals, respectively, and σ_{xy} the covariance. c_1 , c_2 are stability constants. SSIM evaluates

the structural similarity of signals, while low SSIM values indicate greater differences between signals.

2.3.6. Signal-to-Noise Ratio (SNR)

The Signal-to-Noise Ratio (SNR) quantifies the ratio of signal strength to noise. Higher SNR values indicate better noise separation. It is computed as:

$$NR = 10 \cdot \log_{10} \left(\frac{\sum_1^N |y_t|^2}{\sum_1^N |y_t - \hat{y}_t|^2} \right) \tag{8}$$

3. RESULTS

The comprehensive analysis of the deep learning-based denoising autoencoder model revealed remarkable performance in noise removal for ECG signals. The model performed effectively during training and testing phases, demonstrating its success through various performance metrics (Table 2). Notably, the R² score of 0.8389 and the Pearson Correlation Coefficient of 0.9202 indicate a strong relationship between predictions and true values. Additionally, the Structural Similarity Index of 0.6784 confirms the model’s success in visual similarity.

Table 2. Model performance metrics and descriptions.

Metric	Value	Description
Mean Squared Error (MSE)	0.0058	Represents the average of the squared prediction errors. A low MSE indicates high model accuracy.
Mean Absolute Error (MAE)	0.0475	The average of the absolute differences between predicted and actual values.
R ² Score	0.8389	Indicates how well the model fits the data. An R ² value close to 1 shows a good fit.
Pearson Correlation Coefficient (R)	0.9202	Reflects a strong relationship between predictions and actual values.
Structural Similarity Index (SSIM)	0.6784	A visual similarity measure, indicating how closely the predictions resemble the actual data.
Signal-to-Noise Ratio (SNR)	13.4840 dB	Indicates the strength of the signal relative to noise. A high SNR signifies low noise levels.

The training and validation loss graphs (Figure 2) reveal a critical aspect of the model's performance. The consistent convergence of both training and validation losses suggests that the model avoids overfitting, maintaining generalizability across different datasets. This stability is crucial for reliable performance in real-world medical signal processing applications.

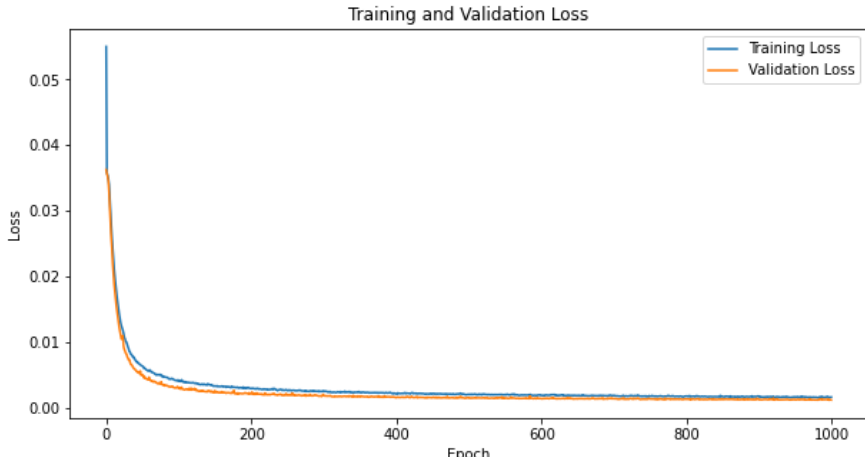


Figure 2. Training and Validation Loss Graphs: A comparison of losses during model training.

Figure 3 provides a compelling visual representation of the model's denoising capabilities. The side-by-side comparison of original, noisy, and denoised signals demonstrates the model's ability to effectively remove noise while preserving the critical morphological features of the ECG signals. The reconstructed signals closely resemble the original signals, with minimal distortion.

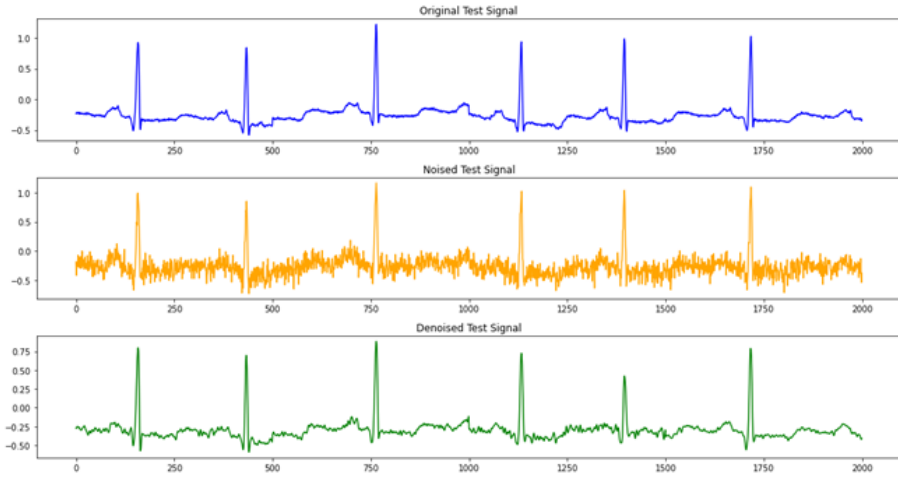


Figure 3. Test Set Signal Examples: Original, noisy, and denoised signal visualizations.

The regression analysis in Figure 4 graphically illustrates the strong correlation between predicted and actual values. The tight clustering of points along the diagonal line indicates high prediction accuracy. Figure 5 further supports this by visualizing the minimal deviations between true and predicted values.

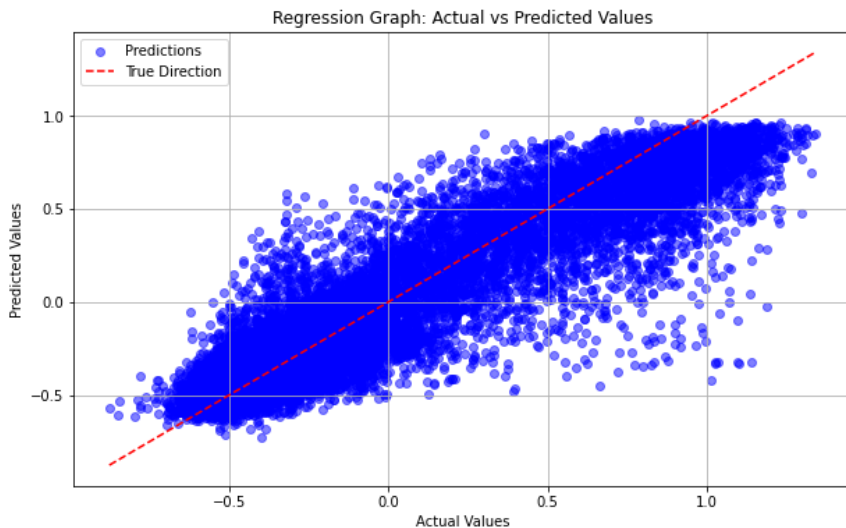


Figure 4. Regression Analysis: Relationship between predicted and actual values.

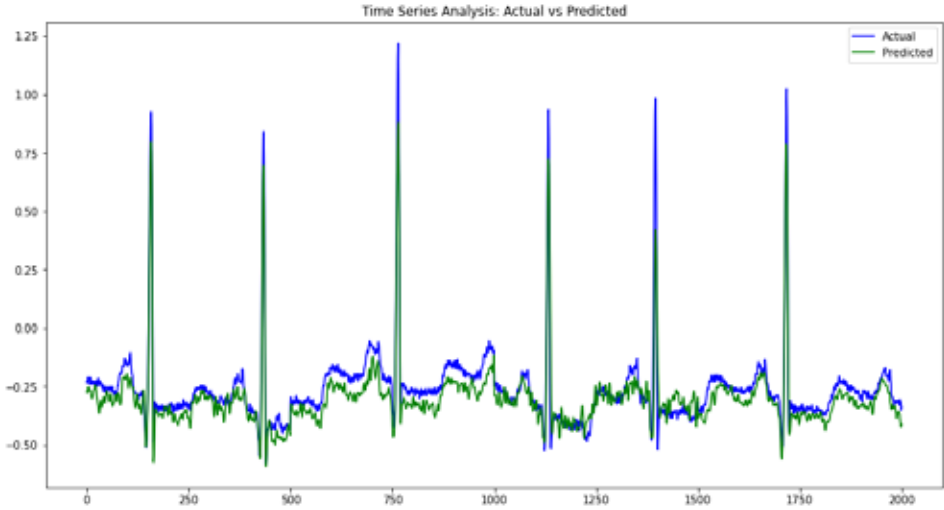


Figure 5. Comparison of True and Predicted Values: Visualizing deviations in predictions.

In conclusion, the developed denoising autoencoder model successfully modeled the complex noise patterns in ECG signals and accurately predicted denoised signals. The model performed well not only in terms of accuracy but also in visual metrics such as SSIM and SNR.

This model can facilitate more accurate analyses by providing clean ECG signals, particularly for diagnosing cardiovascular diseases. Furthermore, the proposed method can be extended to other biomedical signals for noise removal.

4. DISCUSSION

The proposed deep learning-based denoising autoencoder represents a significant advancement in ECG signal processing, addressing critical challenges in noise removal that have long plagued traditional filtering techniques. By leveraging sophisticated neural network architectures, the study demonstrates a novel approach to managing the complex noise environments inherent in medical signal acquisition.

Comparative analysis reveals that the model performs superiorly compared to conventional filter-based methods. Traditional techniques like low-pass, high-pass, and band-pass filters often struggle with multi-source noise and non-

stationary signal characteristics. In contrast, the deep learning approach exhibits remarkable adaptability in noise pattern recognition and signal reconstruction. The encoder-decoder architecture enables the model to transform noisy signals into a lower-dimensional latent representation, effectively separating meaningful cardiac electrical information from noise interference.

The high performance across various metrics carries substantial implications for cardiovascular diagnostics. Clean, noise-free ECG signals are paramount for accurate interpretation of cardiac conditions. By providing a robust method for noise removal, this model can potentially enhance diagnostic accuracy, reduce misinterpretation risks, and support more reliable patient care. The ability to reconstruct signals with minimal distortion opens new avenues for more precise medical signal analysis.

Despite the promising results, several methodological limitations require acknowledgment. The current study primarily used artificially generated noise, which may not fully capture the complexity of real-world noise sources. While comprehensive, this approach represents a controlled environment that might not entirely reflect the unpredictable nature of clinical signal acquisition. Future research should incorporate more diverse, real-world noisy signals to enhance model robustness and generalizability.

The research contributes significantly to the growing body of knowledge in deep learning applications for medical signal processing. The proposed methodology demonstrates the potential of neural network architectures, specifically denoising autoencoders, in handling complex signal processing challenges. The study not only provides a novel approach to ECG signal denoising but also sets a foundational framework for exploring similar techniques in other biomedical signal domains.

The model's current implementation suggests promising avenues for future research. Extending the noise removal techniques to other biomedical signals such as EEG, EMG, or neural recordings represents a potentially transformative research direction. Additionally, future iterations could explore more advanced neural network architectures, implement transfer learning techniques, or develop ensemble methods to further improve performance and generalizability.

Methodologically, the study underscores the importance of comprehensive evaluation metrics. By utilizing multiple performance indicators including Mean Squared Error, Pearson Correlation, Structural Similarity Index, and Signal-

to-Noise Ratio, the research provides a holistic assessment of the model's capabilities. This multi-faceted approach ensures a robust and credible evaluation of the proposed denoising technique.

In conclusion, the developed denoising autoencoder model represents a significant step forward in medical signal processing. By providing a sophisticated, data-driven approach to noise removal, this research opens new possibilities for more accurate and reliable biomedical signal analysis. The potential impact extends beyond immediate clinical applications, suggesting a broader transformation in how we approach signal processing challenges in medical technologies.

REFERENCES

- Antczak, K. (2018). Deep recurrent neural networks for ECG signal denoising. arXiv preprint arXiv:1807.11551.
- Arsene, C. T., Hankins, R., & Yin, H. (2019, September). Deep learning models for denoising ECG signals. In 2019 27th European Signal Processing Conference (EUSIPCO) (pp. 1-5). IEEE.
- Bakurov, I., Buzzelli, M., Schettini, R., Castelli, M., & Vanneschi, L. (2022). Structural similarity index (SSIM) revisited: A data-driven approach. *Expert Systems with Applications*, 189, 116087.
- Castells, F., Laguna, P., Sörnmo, L., Bollmann, A., & Roig, J. M. (2007). Principal component analysis in ECG signal processing. *EURASIP Journal on Advances in Signal Processing*, 2007, 1-21.
- Chai, T., & Draxler, R. R. (2014). Root mean square error (RMSE) or mean absolute error (MAE). *Geoscientific model development discussions*, 7(1), 1525-1534.
- Chatterjee, S., Thakur, R. S., Yadav, R. N., Gupta, L., & Raghuvanshi, D. K. (2020). Review of noise removal techniques in ECG signals. *IET Signal Processing*, 14(9), 569-590.
- Fotiadou, E., & Vullings, R. (2020). Multi-channel fetal ECG denoising with deep convolutional neural networks. *Frontiers in Pediatrics*, 8, 508.
- Joshi, S. L., Vatti, R. A., & Tornekar, R. V. (2013, April). A survey on ECG signal denoising techniques. In 2013 International Conference on Communication Systems and Network Technologies (pp. 60-64). IEEE.
- Kingma, D. P. (2014). Adam: A method for stochastic optimization. arXiv preprint

arXiv:1412.6980.

- Moody, G. B., & Mark, R. G. (2001). The impact of the MIT-BIH arrhythmia database. *IEEE engineering in medicine and biology magazine*, 20(3), 45-50.
- Ruppert, D. (2004). *The elements of statistical learning: data mining, inference, and prediction*.
- Sameni, R., Shamsollahi, M. B., & Jutten, C. (2006, September). Multi-channel electrocardiogram denoising using a bayesian filtering framework. In *2006 Computers in Cardiology* (pp. 185-188). IEEE.
- Sayadi, O., & Shamsollahi, M. B. (2008). ECG denoising and compression using a modified extended Kalman filter structure. *IEEE transactions on biomedical engineering*, 55(9), 2240-2248.
- Vincent, P., Larochelle, H., Bengio, Y., & Manzagol, P. A. (2008, July). Extracting and composing robust features with denoising autoencoders. In *Proceedings of the 25th international conference on Machine learning* (pp. 1096-1103).
- Vincent, P., Larochelle, H., Lajoie, I., Bengio, Y., Manzagol, P. A., & Bottou, L. (2010). Stacked denoising autoencoders: Learning useful representations in a deep network with a local denoising criterion. *Journal of machine learning research*, 11(12).
- Xiong, P., Wang, H., Liu, M., & Liu, X. (2015). Denoising autoencoder for electrocardiogram signal enhancement. *Journal of Medical Imaging and Health Informatics*, 5(8), 1804-1810.
- Zhang, C., Li, X., & Zhang, M. (2010, June). A novel ECG signal denoising method based on Hilbert-Huang Transform. In *2010 International Conference on Computer and Communication Technologies in Agriculture Engineering* (Vol. 2, pp. 284-287). IEEE.

CHAPTER 2

MOLECULAR DOCKING STUDIES OF ANTIDIABETIC COMPOUNDS WITH DPPIV PROTEASE

Assoc.Prof. Dr. Alev ER

Istanbul University

Science Faculty, Physics Department

ORCID NO: 0000-0002-3190-5342

Prof. Dr. Sefa CELIK

Istanbul University

Science Faculty, Physics Department

ORCID NO: 0000-0001-6216-1297

INTRODUCTION

Metabolic disease, known as type 2 diabetes mellitus (T2DM), is caused by the body's production of inadequate amounts of insulin. Drugs that control blood glucose levels by either lowering the synthesis of liver glycogen or enhancing insulin secretion are used to treat it. Dipeptidyl peptidase IV inhibitors (DPPIV), sodium/glucose cotransporter 2 inhibitors (SGLT2), sulfonylurea receptor modulators (SUR), peroxisome proliferator-activated receptor γ agonists (PPAR γ), and other substances are the primary targets of these medications (Guo et al., 2024). T2DM is now widely believed to be an adult illness linked to obesity and cardiac issues, as opposed to diabetes mellitus (T1DM), which initially manifests in childhood as a result of inadequate insulin production. In addition to Europe, Asia, and subsequently South America (in the 1600s), its symptoms were noted in antiquity. Due to the removal of significant quantities of

glucose from the urine, “sweet urine” was the diagnosis in each case (Newman, 2024).

By 2045, there will likely be 783 million diabetics globally, according to the International Diabetes Federation (IDF). Chronic energy excess, such as obesity (absolute energy excess) and aging (relative energy excess), is a significant risk factor for type 2 diabetes, even though the disease has many contributing causes, including genetic and environmental factors. Currently, metabolic surgery, medicine, and lifestyle changes are used to prevent and cure type 2 diabetes. However, because of the shortcomings in the effectiveness and adverse effects of current medications, there is a high need for the creation of new ones. Finding new therapeutic targets is essential to enhancing the treatment of type 2 diabetes (Sun et al., 2022; Zheng et al., 2018; Le et al., 2024).

The metabolic disease with the greatest death rate is diabetes. The pathogenic elements that contribute to the development of diabetes, including receptors, enzymes, genes, and proteins, are targeted by oral antidiabetic medications. The potential of sodium-glucose co-transporters (SGLTs) to successfully treat Type 2 diabetes mellitus has recently come to light. The two types of SGLTs are SGLT-1 and SGLT-2, with SGLT-2 being a crucial transporter in the reabsorption of glucose. Consequently, SGLT inhibitors could be a wise option for blood glucose regulation. SGLT-2 inhibitors include dapagliflozin and canagliflozin (Kumar et al., 2020). In diabetics with chronic kidney disease (CKD), inhibition of sodium-glucose cotransporter 2 (SGLT2) is beneficial in lowering plasma glucose and hemoglobin A1c (HbA1c). It has also been shown to be useful against type 2 diabetes. Recently licensed for the treatment of type 2 diabetes, bexagliflozin is an oral SGLT2 inhibitor that has shown potential in the battle against chronic kidney disease. The structural difference between bexagliflozin and other SGLT2 inhibitors is the presence of a cyclopropyloxyethoxy group at the para position of the peripheral phenyl ring (Bassett et al., 2024). Type 2 diabetes mellitus (T2DM) can be treated with canagliflozin, an inhibitor of the sodium glucose-cotransporter (SGLT) receptor. According to a 2019 research, canagliflozin decreased composite cardiovascular outcomes including non-fatal myocardial infarction, non-fatal stroke, and cardiovascular mortality (Jakher et al., 2019).

DPP-4i and SGLT2i together provide complementary glucose-lowering effects in T2D patients, are safe, and do not result in hypoglycemia. For individuals receiving diet and exercise treatment or who are currently receiving metformin, dual therapy is more beneficial than monotherapy (Scheen, 2016).

Inhibitors of dipeptidyl peptidase-4 (DPP4) provide novel approaches to the management of type 2 diabetes (T2DM). Linagliptin is the first DPP4 inhibitor with a non-renal route of elimination and differs from previously marketed DPP4 inhibitors in its pharmacokinetic characteristics and pharmacodynamic profile in clinical practice. Consequently, in individuals with renal impairment, it can be given without dosage modification or renal function monitoring (Scheen, 2011).

A new hypoglycemic medication called bexagliflozin is a potent SGLT2 inhibitor that is being created to control glycemia in type 2 diabetes. On January 20, 2023, bexagliflozin received initial clearance from the US Food and Drug Administration (USFDA) to be used in conjunction with exercise and lifestyle modifications as an adjuvant therapy agent for type 2 diabetes. In T2DM, bexagliflozin 20 mg dramatically lowers body weight, glycemic impact, HbA1c, and additional glycemic effect compared to the placebo arm (Dholariya et al., 2023).

Dapagliflozin is a favorable, safe, and helpful drug for people with type 2 diabetes because it dramatically lowers glucose reabsorption, which lowers blood glucose levels without the need for insulin. A decrease in body weight has also been linked to dapagliflozin's inhibition of glucose reabsorption (Filippatos et al., 2015). Inhibition of DPP4 protease (PDBID:1X70) activity using DPP4 inhibitors also causes several biological effects in peripheral tissues (Mathur et al., 2023).

Bexagliflozin, Canagliflozin, Dapagliflozin, and Linagliptin's binding energies with dipeptidyl peptidase IV receptor were calculated separately using molecular docking analysis.

1. METHODS AND CALCULATIONS

The conformer was subjected to the energy minimization process of the YASARA structure program (Krieger et al., 2014) using the NOVA force field (Krieger et al., 2002), and the energy-minimized Linagliptin, Dapagliflozin, Canagliflozin, and Bexagliflozin molecules were used as input for the docking simulation. Furthermore, the receptor (PDB ID: 1X70) (Kim et al., 2005) were subjected to the YASARA structure program's energy minimization process using the NOVA force field before the docking simulations. The VINA docking

approach (Trott et al., 2010) and the YASARA software (v22.9.24) were used to study molecular docking. The target receptor was prepared for docking once the ligands and water molecules were eliminated from the PDB data and polar hydrogen atoms were added. The Kollman charges of the target were determined. The docking simulations were carried out using a semi-flexible docking process.

2. RESULTS

Bexagliflozin, Canagliflozin, Dapagliflozin, and Linagliptin complexes docked with DPPIV were shown to have binding energies of -6.61 kcal/mol, -8.341 kcal/mol, -7.501 kcal/mol, and -8.789 kcal/mol, respectively. **Figures 1-4** show 3D docking representations of the bexagliflozin, canagliflozin, dapagliflozin, and linagliptin complexes in the DPPIV active site.

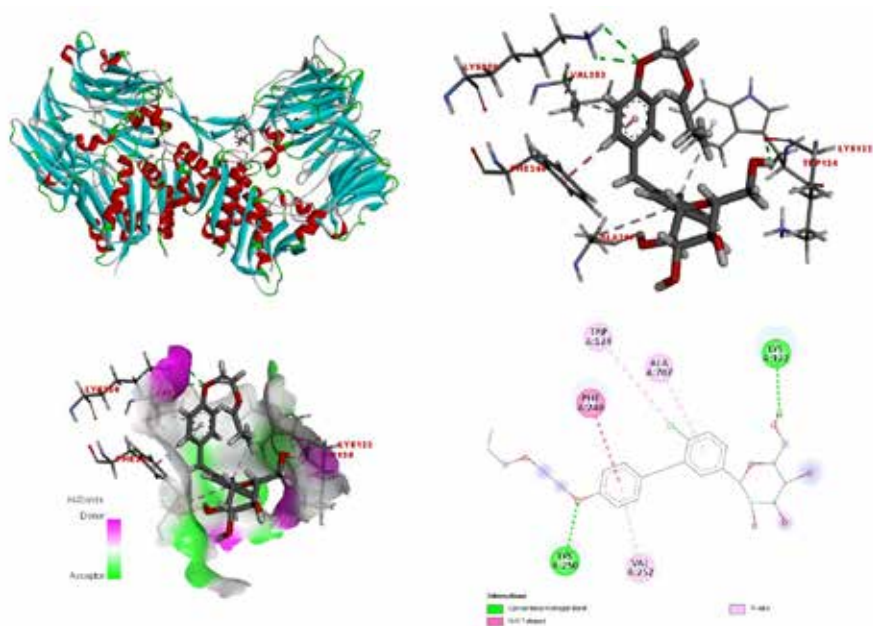


Figure 1. In the molecular docked model of Bexagliflozin with DPPIV (PDB ID: 1X70), the interactions between the Bexagliflozin and DPPIV are labeled using colored dashed lines (binding energy -6.61 kcal/mol).

The interactions found by calculation between the DPPiV protease (PDB ID: 1X70) and Bexagliflozin are as follows;

- 2.26 Å long hydrogen bond with LYS122;
- 4.67 Å long pi-alkyl interaction with TRP124;
- 5.03 Å long pi-pi t-shaped interaction with PHE240;
- 2.34 and 2.67 Å lengths hydrogen bonds with LYS250;
- 3.88 Å long pi-alkyl interaction with VAL252;
- 5.18 Å long pi-alkyl interaction with ALA707.

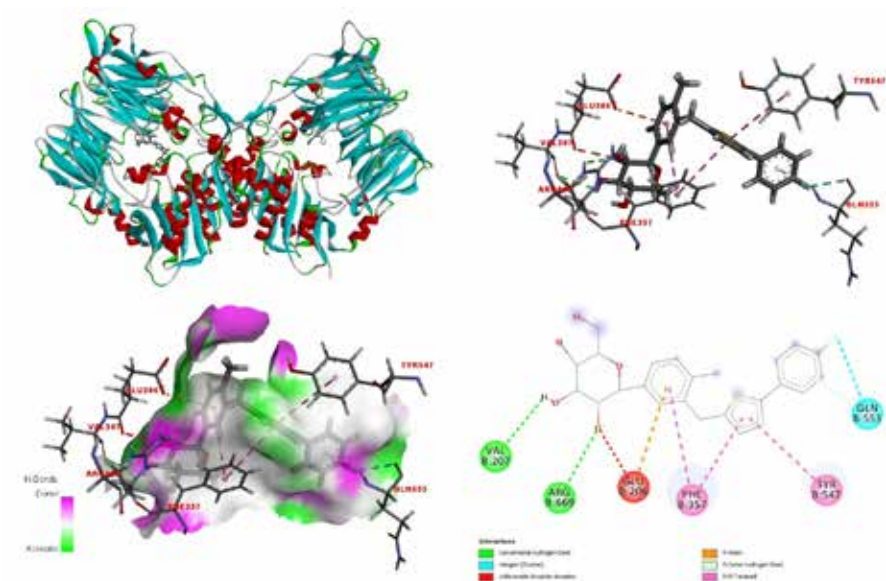


Figure 2. In the molecular docked model of Canagliflozin with DPPiV (PDB ID: 1X70), the interactions between the Canagliflozin and DPPiV are labeled using colored dashed lines (binding energy -8.341 kcal/mol).

The interactions found by calculation between the DPPiV protease (PDB ID: 1X70) and Canagliflozin are as follows;

- 4.24 Å long pi-anion interaction and 2.81 Å long unfavorable acceptor-acceptor interaction with GLU206;
- 2.91 Å long hydrogen bond with VAL207;
- 4.74 and 5.16 Å lengths pi-pi t-shaped interactions with PHE357;

- 5.06 Å long pi-pi t-shaped interaction with TYR547;
- 2.92 Å pi-donor hydrogen bond interaction and 2.98 Å halogen (fluorine) interaction with GLN553;
- 3 Å long hydrogen bond with ARG669.

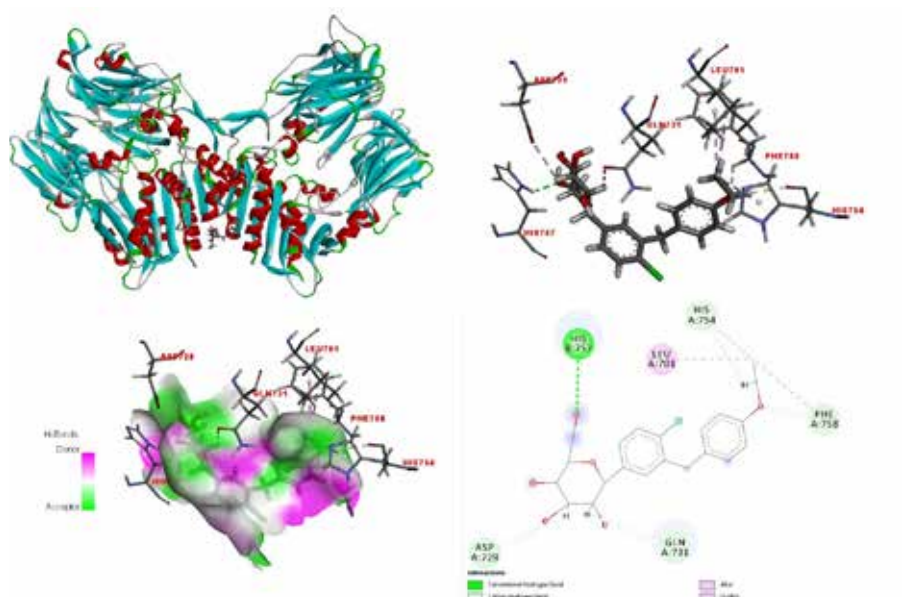


Figure 3. In the molecular docked model of Dapagliflozin with DPPIV (PDB ID: 1X70), the interactions between the Dapagliflozin and DPPIV are labeled using colored dashed lines (binding energy -7.501 kcal/mol).

The interactions found by calculation between the DPPIV protease (PDB ID: 1X70) and Dapagliflozin are as follows;

- 4.05 Å long alkyl interaction with LEU701;
- 3.08 Å long carbon hydrogen bond interaction with ASP729;
- 2.96 Å long carbon hydrogen bond interaction with GLN731;
- 2.27 Å long carbon hydrogen bond interaction and 3.88 Å long pi-alkyl interaction with HIS754;
- 2.46 Å long hydrogen bond with HIS757;
- 2.83 Å long carbon hydrogen bond interaction and 4.84 Å long pi-alkyl interaction with PHE758.

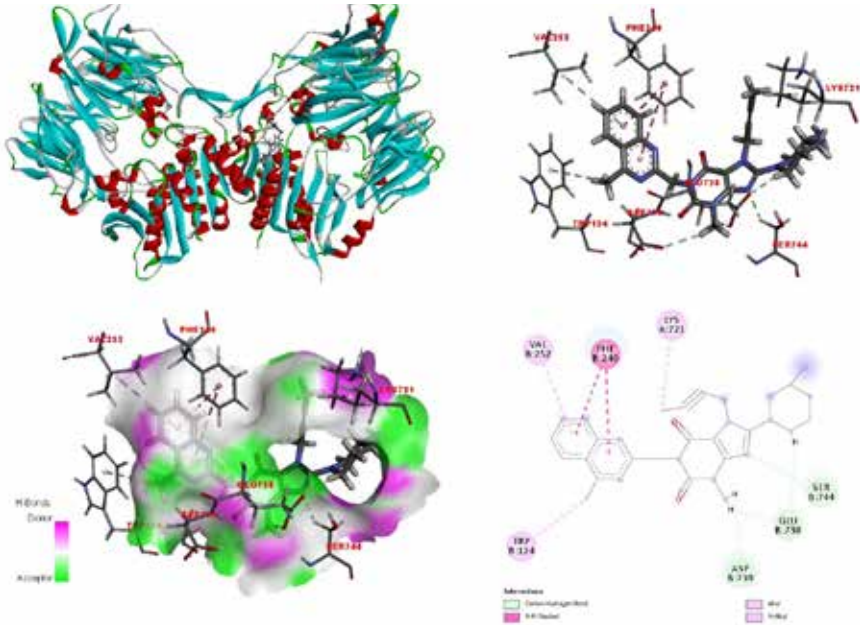


Figure 4. In the molecular docked model of Linagliptin with DPPiV (PDB ID: 1X70), the interactions between the Linagliptin and DPPiV are labeled using colored dashed lines (binding energy -8.789 kcal/mol).

The interactions found by calculation between the DPPiV protease (PDB ID: 1X70) and Linagliptin are as follows;

- 4.9 Å long pi-alkyl interaction with TRP124;
- 4.32 and 5.56 Å long pi-pi stacked interactions with PHE240;
- 5.03 Å long pi-alkyl interaction with VAL252;
- 5.37 Å long alkyl interaction with LYS721;
- 2.39 and 2.58 Å lengths carbon hydrogen bonds with GLU738;
- 2.94 Å long carbon hydrogen bond with ASP739;
- 2.41 Å long carbon hydrogen bond with SER744.

CONCLUSIONS

Bexagliflozin, Canagliflozin, Dapagliflozin, and Linagliptin are used to prevent and treat type 2 diabetes and control insulin levels. To investigate the mechanism of action, molecular docking simulations of these compounds with DPPIV protease (PDB ID: 1X70) were determined. The results of molecular docking simulations of Bexagliflozin, Canagliflozin, Dapagliflozin, and Linagliptin complexes showed that they have strong binding energies of -6.61 kcal/mol, -8.341 kcal/mol, -7.501 kcal/mol, and -8.789 kcal/mol, respectively. As a result of molecular docking calculations, these molecules can be seen as a solution in the prevention and treatment of type 2 diabetes, which is of great importance today.

REFERENCES

- Bassett, R. L., Gallo, G., Le, K. P. N., & Volino, L. R. (2024). Bexagliflozin: a comprehensive review of a recently approved SGLT2 inhibitor for the treatment of type 2 diabetes mellitus. *Medicinal Chemistry Research*, 33(8), 1354-1367.
- Dholariya, S., Dutta, S., Singh, R., Parchwani, D., Sonagra, A., & Kaliya, M. (2023). Bexagliflozin, a sodium-glucose cotransporter 2 (SGLT2) inhibitor, for improvement of glycemia in type 2 diabetes mellitus: a systematic review and meta-analysis. *Expert Opinion on Pharmacotherapy*, 24(18), 2187-2198.
- Filippatos, T. D., Liberopoulos, E. N., & Elisaf, M. S. (2015). Dapagliflozin in patients with type 2 diabetes mellitus. *Therapeutic advances in endocrinology and metabolism*, 6(1), 29-41.
- Guo, Y. Y., Zhang, J. Y., Sun, J. F., & Gao, H. (2024). A comprehensive review of small-molecule drugs for the treatment of type 2 diabetes mellitus: Synthetic approaches and clinical applications. *European Journal of Medicinal Chemistry*, 116185.
- Jakher, H., Chang, T. I., Tan, M., & Mahaffey, K. W. (2019). Canagliflozin review—safety and efficacy profile in patients with T2DM. *Diabetes, metabolic syndrome and obesity: targets and therapy*, 209-215.
- Kim, D., Wang, L., Beconi, M., Eiermann, G. J., Fisher, M. H., & He, H. (2005). Gerard

- J. Hickey, Jennifer E. Kowalchick, Barbara Leiting, Kathryn Lyons, Frank Marsilio, Margaret E. McCann, Reshma A. Patel, Aleksandr Petrov, Giovanna Scapin, Sangita B. Patel, Ranabir Sinha Roy, Joseph K. Wu, Matthew J. Wyvratt, Bei B. Zhang, Lan Zhu, Nancy A. Thornberry, and Ann E. Weber. *J. Med. Chem.*, 48, 141-151.
- Krieger, E., Koraimann, G., Vriend, G. (2002) Increasing the precision of comparative models with YASARA NOVA—a self-parameterizing force field, *Proteins: Structure, Function, and Bioinformatics*, 47(3), 393-402.
- Krieger, E., Vriend, G. (2014) YASARA View—molecular graphics for all devices—from smartphones to workstations, *Bioinformatics*, 30(20), 2981-2982.
- Kumar, S., Khatik, G. L., & Mittal, A. (2020). Recent developments in sodium-glucose co-transporter 2 (SGLT2) inhibitors as a valuable tool in the treatment of type 2 diabetes mellitus. *Mini Reviews in Medicinal Chemistry*, 20(3), 170-182.
- Le, J., Chen, Y., Yang, W., Chen, L., & Ye, J. (2024). Metabolic basis of solute carrier transporters in treatment of type 2 diabetes mellitus. *Acta Pharmaceutica Sinica B*, 14(2), 437-454.
- Mathur, V., Alam, O., Siddiqui, N., Jha, M., Manaihiya, A., Bawa, S., ... & Shakeel, F. (2023). Insight into structure activity relationship of DPP-4 inhibitors for development of antidiabetic agents. *Molecules*, 28(15), 5860.
- Newman, D. J. (2024). Non-Insulin-Based Drug Entities Used to Treat Diabetes Type 2 Disease (T2DM), Based on Natural Products from All Sources. *Journal of Natural Products*, 87(3), 629-637.
- Scheen, A. J. (2011). Linagliptin for the treatment of type 2 diabetes (pharmacokinetic evaluation). *Expert Opinion on Drug Metabolism & Toxicology*, 7(12), 1561-1576.
- Scheen, A. J. (2016). DPP-4 inhibitor plus SGLT-2 inhibitor as combination therapy for type 2 diabetes: from rationale to clinical aspects. *Expert opinion on drug metabolism & toxicology*, 12(12), 1407-1417.
- Sun, H., Saeedi, P., Karuranga, S., Pinkepank, M., Ogurtsova, K., Duncan, B. B., ... & Magliano, D. J. (2022). IDF Diabetes Atlas: Global, regional and country-level diabetes prevalence estimates for 2021 and projections for 2045. *Diabetes research and clinical practice*, 183, 109119.
- Trott, O., Olson, A. J. (2010) AutoDock Vina: improving the speed and accuracy of docking with a new scoring function, efficient optimization, and multithreading,

Journal of computational chemistry, 31(2), 455-461.

Zheng, Y., Ley, S. H., & Hu, F. B. (2018). Global aetiology and epidemiology of type 2 diabetes mellitus and its complications. *Nature reviews endocrinology*, 14(2), 88-98.

CHAPTER 3

THEORETICAL FRAMEWORK FOR MOLECULAR DOCKING OF SOTORASIB AND REPOTRECTINIB WITH EGFR RECEPTORS

Prof. Dr. Sefa CELIK

Istanbul University

Science Faculty, Physics Department

ORCID NO: 0000-0001-6216-1297

Prof. Dr. Aysen E. OZEL

Istanbul University

Science Faculty, Physics Department

ORCID NO: 0000-0002-8680-8830

INTRODUCTION

About 1.2 million new instances of lung cancer were reported in 2000, making it the most common type of cancer worldwide, making up 12.3% of all cancer cases (Parkin et al., 2001). The main cause of lung cancer, accounting for 80% to 90% of occurrences, is tobacco use, which mostly affects cigarette smokers. There are notable differences in occurrence between genders, racial groups, and geographic regions. Furthermore, some research indicates that after being exposed to toxins in tobacco smoke, women may show an increased risk of developing lung cancer. Individuals who smoke throughout their lifetime have a 20- to 30-fold higher risk of developing lung cancer compared to lifelong

nonsmokers. Although smoking prevalence is declining in the United States, an epidemic of smoking persists in regions such as China and Eastern Europe, which is projected to result in tens of millions of new lung cancer cases during this century (Parkin et al., 2001; Peto et al., 1999; 2000). Consequently, lung cancer is considered the most preventable form of cancer, with smoking cessation significantly reducing the risk after a lag period of approximately seven years (Peto et al., 1999).

Although the risk of lung cancer decreases with smoking cessation, it does not return to baseline levels, and lung cancer in the United States is increasingly becoming a disease predominantly affecting former smokers. Despite advances in therapeutic approaches, the prognosis remains poor, with approximately 90% of lung cancer patients succumbing to the disease. In 2000, lung cancer accounted for an estimated 1.1 million deaths worldwide, representing 17.8% of all cancer-related fatalities. Notably, only approximately 11% of heavy cigarette smokers ultimately develop lung cancer, suggesting the involvement of genetic predisposition as a contributing factor to lung cancer risk (Lippman and Spitz, 2001).

Segregation studies indicate that a familial history of lung cancer correlates with a 2.5-fold heightened risk, independent of cigarette smoking, implying the presence of a rare autosomal dominant gene that predisposes individuals to lung cancer (Amos et al., 1999). This familial association is most prominently observed in lung cancer cases among nonsmokers. However, the majority of inherited risk for lung cancer is likely attributable to the cumulative influence of common genetic polymorphisms, which exert small but significant effects and are widely distributed in the population (Amos et al., 1999; Minna et al., 2002).

Sotorasib is an inhibitor targeting the RAS GTPase family, under development by Amgen for the treatment of solid tumors harboring KRAS G12C mutations. In June 2019, FDA designated sotorasib as an orphan drug for the treatment of KRAS G12C-positive NSCLC and colorectal cancer (Eisenhauer et al., 2009; Cox et al., 2014; Fernández-Medarde et al., 2011; Stephen et al., 2014). Subsequently, the FDA granted breakthrough therapy designation to sotorasib in December 2020 for advanced or metastatic KRAS G12C-mutated NSCLC (Nakajima et al., 2022). Sotorasib was initially approved in the US on 28 May 2021 for use in adults to treat KRASG12C mutation-positive locally advanced or metastatic NSCLC, as identified by an FDA-approved test, based on their status and following at least one previous systemic therapy (Blair, 2021; Nakaji-

ma et al., 2022). Sotorasib irreversibly inhibits GTPase protein of KRASG12C. The efficacy and safety of sotorasib in patients previously treated with KRASG12C-mutated NSCLC were assessed (de Langen et al., 2023).

Repotrectinib is a next-generation multikinase inhibitor targeting ROS1, ALK, and TRK (TRKA/B/C) fusion proteins. It is currently under investigation in an ongoing first-in-human Phase 1/2 clinical trial (NCT03093116). The drug exhibits a high central nervous system exposure and is specifically designed to overcome both wild-type and solvent-front mutations in the target kinases. Potency against resistance mutations like ROS1-G2032R, ROS1-D2033N, TRKA-G595R, TRKB-G639R, TRKC-G623R, and ALK-G1202R are shown. A patient with MASC presenting with lung metastases harboring the *ETV6–NTRK3* fusion was enrolled into a clinical trial investigating entrectinib. The patient achieved a partial response to entrectinib lasting 6 months, after which disease progression occurred. Upon progression, treatment was switched to doxorubicin and then a combination of entrectinib and trametinib, given for 2 months but showed progressive disease during this combination treatment. According to rebiopsy investigations, the tumor developed a unique *NTRK3-G623E* resistance mutation. After that, he was added to a clinical trial that was testing 40 mg of repotrectinib daily. During the first several weeks of treatment, a rapid and pronounced therapeutic response to repotrectinib was observed (Drilon et al., 2018; Salgia, 2019).

The selection of PDB IDs 2ITY and 3W2O for docking studies targeting lung cancer is grounded in the pivotal role of EGFR mutations in the pathogenesis of the disease and the potential interactions of these mutations with therapeutic compounds. PDB ID 2ITY represents the EGFR kinase domain bound to Iressa (Gefitinib), a tyrosine kinase inhibitor (TKI) widely used in the treatment of NSCLC with specific EGFR mutations. PDB ID 3W2O corresponds to the EGFR kinase domain harboring the T790M and L858R mutations in complex with TAK-285. These mutations are particularly relevant in NSCLC, with the L858R mutation enhancing EGFR kinase activity and the T790M mutation conferring resistance to first-generation EGFR inhibitors, such as Gefitinib (Kumar et al., 2024). Sotorasib and Repotrectinib's interactions with EGFR receptors were evaluated separately using molecular docking simulations.

METHODS AND CALCULATIONS

Using the NOVA force field (Krieger et al., 2002), the conformer was sent through the YASARA structure program's energy minimization process (Krieger et al., 2014). The docking simulation was then run using the energy-minimized Sotorasib and Repotrectinib molecules as input. Additionally, prior to docking simulations, the receptors from the protein databank (PDB IDs: 2ITY and 3W2O) (Yun et al., 2007; Sogabe et al., 2013) underwent the YASARA structure program's energy minimization process using the NOVA force field. Molecular docking was studied using the YASARA software (v22.9.24) and the VINA (Trott et al., 2010) docking technique. After removing the ligands and water molecules from the PDB files and adding polar hydrogen atoms, the downloaded target protein was ready for docking. The target's Kollman charges were established. The default settings for the other parameters were used. A semi-flexible docking procedure was used to conduct the docking simulations, maintaining the target protein's rigidity while maintaining the ligand's flexibility.

RESULTS AND DISCUSSIONS

Through the calculation of molecular docking, Sotorasib has a binding energy with the EGFR kinase domain of -8.952 kcal/mol. The three-dimensional model of Sotorasib in complex with the active site of 2ITY is illustrated in **Figure 1**.

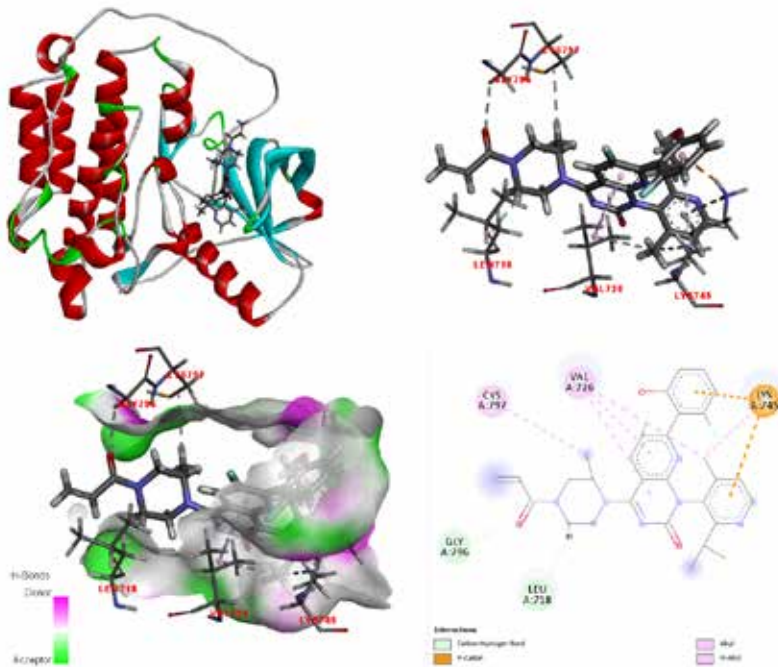


Figure 1. The molecular docking model of Sotorasib with the EGFR kinase domain (PDB ID: 2ITY) highlights the interactions between Sotorasib and the kinase, represented by colored dashed lines. The binding energy of the complex was calculated to be -8.952 kcal/mol.

The specific interactions observed between the EGFR kinase (PDB ID: 2ITY) and Sotorasib are as follows:

LEU718 forms a carbon-hydrogen bond at a distance of 2.6 Å;

VAL726 forms π -alkyl interactions at distances of 4.15 Å and 5.11 Å, as well as an alkyl interaction at a distance of 4.81 Å;

LYS745 forms an alkyl interaction at a distance of 4.27 Å, a π -alkyl interaction at a distance of 4.35 Å, a π -cation: π -donor hydrogen bond interaction at a distance of 2.46 Å, and a π -cation interaction at a distance of 4.55 Å;

GLY796 forms a carbon-hydrogen bond at a distance of 2.85 Å;

CYS797 forms an alkyl interaction at a distance of 4.09 Å.

The molecular docking calculations revealed that the binding energy of Repotrectinib with the EGFR kinase domain (PDB ID: 2ITY) was -8.13 kcal/

mol. The three-dimensional representation of Repotrectinib within the active site of 2ITY is depicted in **Figure 2**.

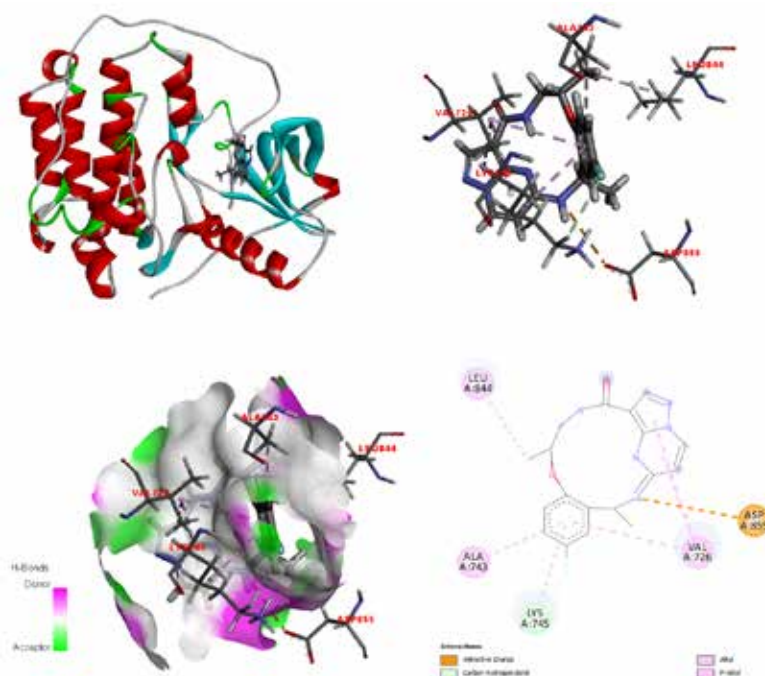


Figure 2. The interactions between Repotrectinib and EGFR kinase (PDB:2ITY) are indicated by colored dashed lines (binding energy -8.13 kcal/mol) in the molecular docked model.

The following are interactions between Repotrectinib and EGFR kinase (PDB ID: 2ITY):

VAL726 forms π -alkyl interactions at distances of 4.49 Å, 4.89 Å, and 4.93 Å;

ALA743 forms a π -alkyl interaction at a distance of 4.9 Å;

LYS745 forms a carbon-hydrogen bond at a distance of 3 Å and a π -alkyl interaction at a distance of 4.39 Å;

LEU844 forms an alkyl interaction at a distance of 4.23 Å;

ASP855 forms an attractive charge interaction at a distance of 4.18 Å.

Sotorasib's binding energy with the EGFR kinase domain carrying the T790M and L858R mutations (PDB ID: 3W2O) was -8.502 kcal/mol, according

to the molecular docking calculations. The three-dimensional representation of Sotorasib within the active site of 3W2O is shown in **Figure 3**.

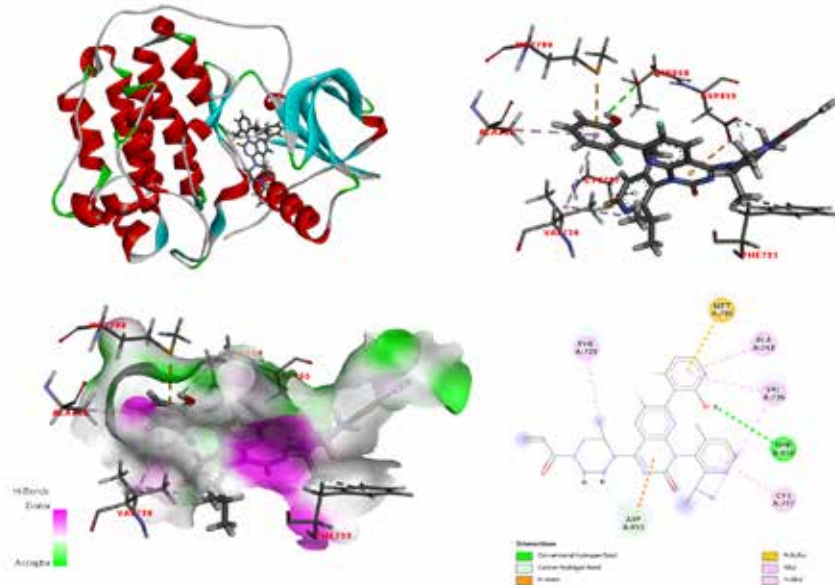


Figure 3. The molecular docking model of Sotorasib with the EGFR kinase domain containing the T790M mutation (PDB ID: 3W2O) illustrates the interactions between Sotorasib and the mutant EGFR kinase domain, represented by colored dashed lines. The binding energy of this complex was calculated to be -8.502 kcal/mol.

The following describes the precise interactions that were noted between sotorasib and the mutant EGFR^{T790M} (PDB ID: 3W2O):

PHE723 interacts with pi-alkyl at 4.64 Å; VAL726 interacts with pi-alkyl at 5.07 Å and alkyl interaction at 5.23 Å; ALA743 interacts with pi-alkyl at 4.90 Å; MET790 interacts with pi-sulfur at 3.85 Å; CYS797 interacts with pi-alkyl at 5.19 Å; THR854 interacts with hydrogen bond at 2.89 Å; ASP855 interacts with pi-anion at 4.08 Å and 2.67, 2.67, and 2.71 Å carbon hydrogen bonds.

The calculations revealed that Repotrectinib's binding energy with 3W2O was -8.215 kcal/mol. **Figure 4** illustrates Repotrectinib's three-dimensional docking representation within the 3W2O active site.

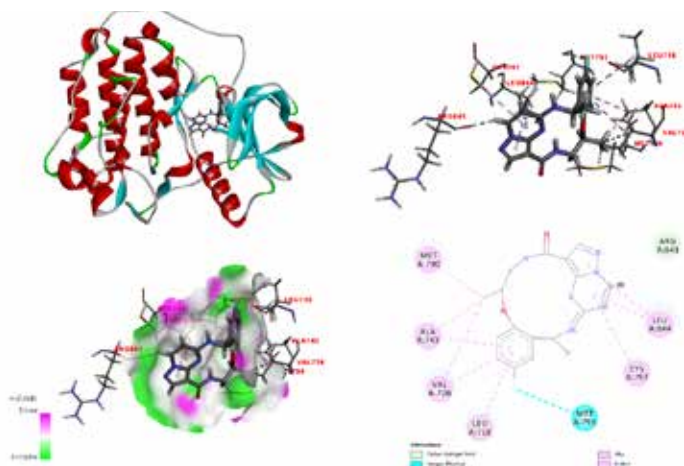


Figure 4. Molecular modeling of repotrectinib with the EGFR-kinase domain by docking using 3W2O. Colored dashed lines indicate the interaction between the EGFR kinase domain and Repotrectinib (binding energy -8.215 kcal/mol).

Repotrectinib and mutant EGFR^{T790M} (PDB ID: 3W2O) interact as follows:
LEU718 forms a π -alkyl interaction at a distance of 5.04 Å;

VAL726 forms an alkyl interaction at a distance of 4.76 Å and a π -alkyl interaction at a distance of 5.14 Å;

ALA734 forms an alkyl interaction at a distance of 3.46 Å and a π -alkyl interaction at a distance of 4.56 Å;

MET790 forms an alkyl interaction at a distance of 4.06 Å;

MET793 forms a halogen (fluorine) interaction at a distance of 3.2 Å;

CYS797 forms a π -alkyl interaction at a distance of 5.08 Å;

ARG841 forms a carbon-hydrogen bond at a distance of 3.1 Å;

LEU844 forms π -alkyl interactions at distances of 5.20 Å and 5.24 Å.

CONCLUSIONS

Non-small cell lung cancer can be treated with sotorasib and repotrectinib. Molecular docking simulations of the compounds' minimized conformation against mutant EGFR^{T790M} (PDB ID: 3W2O) and EGFR kinase (PDB ID: 2ITY) were performed in order to examine the mechanism of action. For the Sotorasib-2ITY, Repotrectinib-2ITY, Sotorasib-3W2O, and Repotrectinib-

3W2O complexes, the corresponding binding energies were determined to be -8.952, -8.13, -8.502, and -8.215 kcal/mol. The calculated high binding energies against mutant EGFR^{T790M} and EGFR kinase indicate that they may be useful in the treatment of lung cancer. Today, studies are intensively continuing to provide the best possible treatment for lung cancer. In this study, it has been investigated that complexes formed by independent docking of satorasib and repotrectinib molecules with EGFR receptors may be drug candidates for the treatment of lung cancer.

REFERENCES

- Amos, C. I., Xu, W., & Spitz, M. R. (1999). Is there a genetic basis for lung cancer susceptibility?. *Chemoprevention of Cancer: A Clinical Update*, 3-12.
- Blair, H. A. (2021). Sotorasib: first approval. *Drugs*, 81(13), 1573-1579.
- Cox, A. D., Fesik, S. W., Kimmelman, A. C., Luo, J., & Der, C. J. (2014). Drugging the undruggable RAS: Mission possible?. *Nature reviews Drug discovery*, 13(11), 828-851.
- de Langen, A. J., Johnson, M. L., Mazieres, J., Dingemans, A. M. C., Mountzios, G., Pless, M., ... & Paz-Ares, L. (2023). Sotorasib versus docetaxel for previously treated non-small-cell lung cancer with KRASG12C mutation: a randomised, open-label, phase 3 trial. *The Lancet*, 401(10378), 733-746.
- Drilon, A., Ou, S. H. I., Cho, B. C., Kim, D. W., Lee, J., Lin, J. J., ... & Shaw, A. T. (2018). Repotrectinib (TPX-0005) is a next-generation ROS1/TRK/ALK inhibitor that potently inhibits ROS1/TRK/ALK solvent-front mutations. *Cancer discovery*, 8(10), 1227-1236.
- Eisenhauer, E. A., Therasse, P., Bogaerts, J., Schwartz, L. H., Sargent, D., Ford, R., ... & Verweij, J. (2009). New response evaluation criteria in solid tumours: revised RECIST guideline (version 1.1). *European journal of cancer*, 45(2), 228-247.
- Fernández-Medarde, A., & Santos, E. (2011). Ras in cancer and developmental diseases. *Genes & cancer*, 2(3), 344-358.
- Krieger, E., Vriend, G. (2014) YASARA View—molecular graphics for all devices—from smartphones to workstations, *Bioinformatics*, 30(20), 2981-2982.
- Krieger, E., Koraimann, G., Vriend, G. (2002) Increasing the precision of comparative models with YASARA NOVA—a self-parameterizing force field, *Proteins: Structure, Function, and Bioinformatics*, 47(3), 393-402.

- Kumar, A., Tiwari, A., & Tiwari, V. (2024). Computational and experimental insights into glycyrrhizin-loaded nanostructured lipid carriers: docking, dynamics, design optimization, and anticancer efficacy in lung cancer cells. *Future Journal of Pharmaceutical Sciences*, 10(1), 164.
- Lippman, S. M., & Spitz, M. R. (2001). Lung cancer chemoprevention: an integrated approach. *Journal of Clinical Oncology: Official Journal of the American Society of Clinical Oncology*, 19(18 Suppl), 74S-82S.
- Minna, J. D., Roth, J. A., & Gazdar, A. F. (2002). Focus on lung cancer. *Cancer cell*, 1(1), 49-52.
- Nakajima, E. C., Drezner, N., Li, X., Mishra-Kalyani, P. S., Liu, Y., Zhao, H., ... & Singh, H. (2022). FDA approval summary: sotorasib for KRAS G12C-mutated metastatic NSCLC. *Clinical Cancer Research*, 28(8), 1482-1486.
- Salgia, R. (Ed.). (2019). *Targeted therapies for lung cancer*. Springer International Publishing.
- Stephen, A. G., Esposito, D., Bagni, R. K., & McCormick, F. (2014). Dragging ras back in the ring. *Cancer cell*, 25(3), 272-281.
- Parkin, D. M., Bray, F. I., & Devesa, S. (2001). Cancer burden in the year 2000. The global picture. *European journal of cancer*, 37, 4-66.
- Peto, R., Chen, Z. M., & Boreham, J. (1999). Tobacco—the growing epidemic. *Nature medicine*, 5(1), 15-17.
- Peto, R., Darby, S., Deo, H., Silcocks, P., Whitley, E., & Doll, R. (2000). Smoking, smoking cessation, and lung cancer in the UK since 1950: combination of national statistics with two case-control studies. *Bmj*, 321(7257), 323-329.
- Sogabe, S., Kawakita, Y., Igaki, S., Iwata, H., Miki, H., Cary, D. R., ... & Ishikawa, T. (2013). Structure-based approach for the discovery of pyrrolo [3, 2-d] pyrimidine-based EGFR T790M/L858R mutant inhibitors. *ACS medicinal chemistry letters*, 4(2), 201-205.
- Trott, O., Olson, A. J. (2010) AutoDock Vina: improving the speed and accuracy of docking with a new scoring function, efficient optimization, and multithreading, *Journal of computational chemistry*, 31(2), 455-461.
- Yun, C. H., Boggon, T. J., Li, Y., Woo, M. S., Greulich, H., Meyerson, M., & Eck, M. J. (2007). Structures of lung cancer-derived EGFR mutants and inhibitor complexes: mechanism of activation and insights into differential inhibitor sensitivity. *Cancer cell*, 11(3), 217-227.

CHAPTER 4

BUSHING TYPES OF POWER TRANSFORMERS

Başak AKİPEK

Istanbul University

Department of Electrical-Electronics Engineering

asak.akipek@gmail.com

Serap CEKLİ

Istanbul University

Department of Electrical-Electronics Engineering

ORCID NO: 0000-0002-8113-0514

Cengiz Polat UZUNOĞLU

Istanbul University

Department of Electrical-Electronics Engineering

polat@iuc.edu.tr

ORCID NO: 0000-0002-4891-3963

INTRODUCTION

Bushings are a critical component in the safe and efficient transport of electricity. They can be located in transformer buildings, switchgear facilities and on transformer tanks. The main purpose of the bushing is to transfer the load currents in and out of the basic enclosures at the voltage of the system. Normal ageing of bushing insulation is usually independent of transformer conditions and can therefore be considered in isolation. If the insulation system of the bushing fails, it may result in fire or injury to personnel. Case studies on different

transformers show how the trend of moisture and dielectric properties changes with the change of power factor and capacitance of the insulation system [1].

During operation, earth short-circuit faults frequently occur in the bushings. Therefore, in order to prevent bushing failures, it is very important to identify the root causes of bushing failures, accurately locate internal faults and understand the fault development process.

It is among the large-scale equipment for the transmission of electrical energy and the adjustment of voltage. The bushing provides both the transfer of the internal energy of the transformer to the outside and the isolation and stabilisation of the high-voltage conductor with the ground [2].

Bushing is a system that allows one or more conductors to pass through a compartment such as a tank and insulates these conductors from the compartment [3].

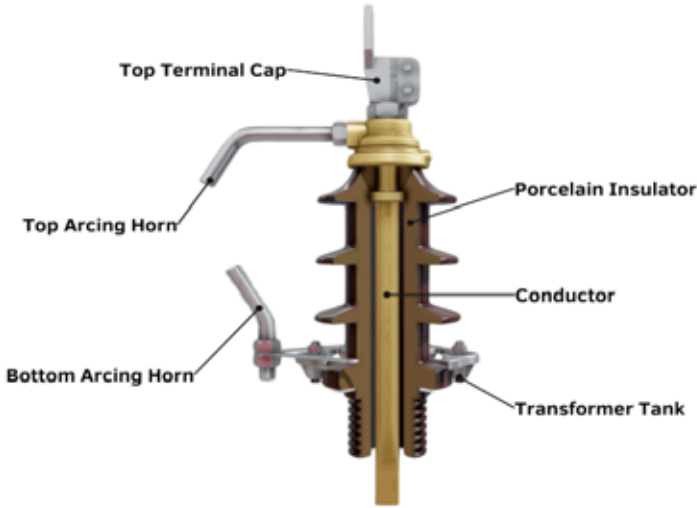
LV and HV winding ends of the transformers are taken out of the tank and are made with the bushings placed on the tank. At voltages below 45 kV, DIN type bushings are generally used, while condenser type bushings are used at voltages above 45 kV [4].

10% of the transformer failures are caused by bushing failures. For this reason, regular measurement and follow-up is of great importance [3].

Losses in transformers may also vary depending on the load. One of these losses is the loss component arising from eddy currents in the tank area around the bushings. This effect is not very important in HV bushings, but it is important in LV bushings since the current is high. The proximity of the LV conductors to the tank also has a significant influence on the load [5].

STRUCTURE OF BUSHINGS

The main purpose of the bushings is to transmit the incoming voltage to the bushing housing. Bushings are HV fittings that serve to take out the energised ends of the transformer and provide isolation from this energised end with the earthed body. Generally, their outer surfaces are made of porcelain and their dimensions vary according to the voltage level at which they are used. Bushings are classified according to the nature of the insulation between the centre conductor and the porcelain part [4].



Oil Filled Porcelain Bulk Bushing

Fig.1 Oil Filled Porcelain Bushing [6].

Bushings create an electric field. As the strength of this electric field increases, leakage current may occur. If this current increases gradually, arcing may occur. The insulation of the bushing can be made of porcelain, paper or resin.

Porcelain Insulation

- It is a bushing that can be used both indoors and outdoors.
- The cost is low.
- Porcelain insulation must be supported by gaskets on the tank. However, oil may leak from the gaskets that harden over time. In this case, it should be checked and maintained frequently.
- The porcelain bushing is hollow inside. It is filled with oil to increase insulation. Usually used up to 35 kV.

Paper insulation

- Paper is a disadvantage as it absorbs moisture, but the dielectric strength of paper insulation is high.
- Paper insulation is impregnated either with oil or resin.

Bushings consist of the condenser body around a centre tube using quality kraft insulation paper. The paper strips are designed for dielectric strength and

are surrounded by aluminium foils [7].

The bushing body, bottom porcelain and welded flange are placed in a durable tank. The space between the bushing body and the tank is filled with transformer oil. It is supported and sealed with gaskets to prevent oil leakage from the parts at the top of the bushing [7].

To observe the oil level, the level is read from the oil level indicator on the expansion tank. The space above the expansion tank is filled with nitrogen gas. Therefore, less maintenance is required [7].

Dry Type Bushings

In dry type bushings, the part between the centre conductor and the outer porcelain is filled with porcelain. It is generally used on the low voltage side and in distribution transformers [4].

Oil type bushings

In this type of bushings, the part between the centre conductor and the outer porcelain is filled with oil. This type of bushing is used in almost all distribution transformers. Up to a certain power, the oil in the transformer tank also fills the inside of the bushing. In large power transformers, the oil placed in the bushing is connected to the expansion tank through thin pipes [4].

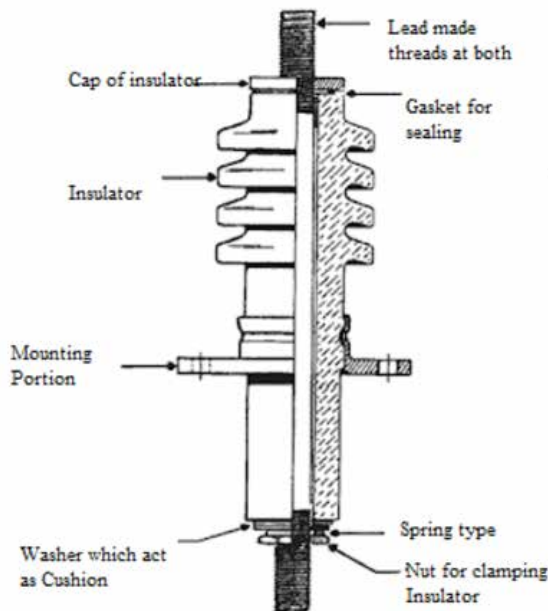


Fig.2 Oil Type Bushing [8].

CONDENSER BUSHING

Condenser bushings are divided into 3 types as OIP (oil-impregnated paper bushing), RBP (resin-bonded paper bushing) and RIP (resin-impregnated paper bushing).

Condenser bushings facilitate electrical voltage control through the placement of floating stabilising screens. The floating stabilising screens are made of conductive material. Since the condenser core will reduce the field gradient and dissipate the field, the screens are distributed coaxially and balance is achieved between internal and external puncture strength. The capacitor core in which the screens are located reduces the field gradient and distributes the field along the length of the insulator. The screens are placed coaxially, providing an optimum balance between external and internal puncture strength [9].

Condenser bushings are designed so that the insulating paper wraps the conductor. Metallic electrodes are also placed inside the winding. In this case, the electric field of the bushing is uniformly distributed. The centre conductor wrapped in insulating paper is impregnated with transformer oil or resin to further increase the dielectric strength [10].

Condenser bushings are designed for long life and minimising failure. Condenser bushings provide a wide range for low partial discharges and overheating when the rated voltage is exceeded. There are types where the outer insulation of the condenser bushings is polymeric or ceramic [10]. The control of voltage, thermal current and mechanical stress is very important in order to be able to design the bushing correctly [10].

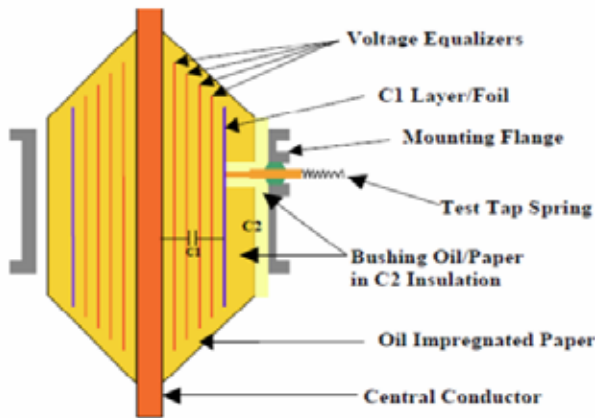
HVDC transformer and wall bushings for 800 kV DC have been developed and verified by extensive short and long term tests. Development bushings for high voltages and complicated applications needs both large facilities and much experience. Operating at high voltage levels causes dielectric heating of the insulation. For this reason, dielectric losses can be neglected at low voltages in a normal bushing, but cannot be neglected at high voltages [10].

The insulating material in the bushing has the lowest dissipation factor at approximately 60 °C and then increases with temperature. There is therefore a limit for a each bushing exists that if passed will result in inadequate heat dissipation and consequently an uncontrolled temperature increase. This phenomenon is known as thermal runaway and can result in failure [10].

The dissipation limit is thermal stability. Both load losses and capacitive losses occur in bushings. Therefore, full stability is required at high voltages. In a properly designed bushing, dielectric losses and rated currents are not critical [10].

The production phase of RIP bushings is more difficult than the production phase of OIP bushings. Because oil impregnation under vacuum is a simpler process to fill the oil into all parts of the bushing. Void-free products must be manufactured carefully [10].

OIP (Oil-Impregnated Paper Bushing)



2 Construction of typical OIP condenser bushing rated ≤ 69 kV[2]

Fig.3 OIP Condenser [11].

OIP type bushings, which are generally used at high voltage, are designed as condenser type by wrapping aluminium foils isolated from each other at certain intervals between paper insulation layers in order to prevent arc and increase puncture resistance [4].

At the point where the winding exits the tank, the voltage distribution between the centre conductor and the earthed flange is not homogeneous. This inhomogeneous distribution forces the isolation of the bushing. Due to the homogenisation of the voltage distribution, the condenser layers divide the capacitive induction voltage, providing a homogeneous voltage and electric field distribution between the centre conductor and the grounded flange. In order to increase the dielectric strength of the insulating paper used, the paper is impregnated with insulating oil [4].

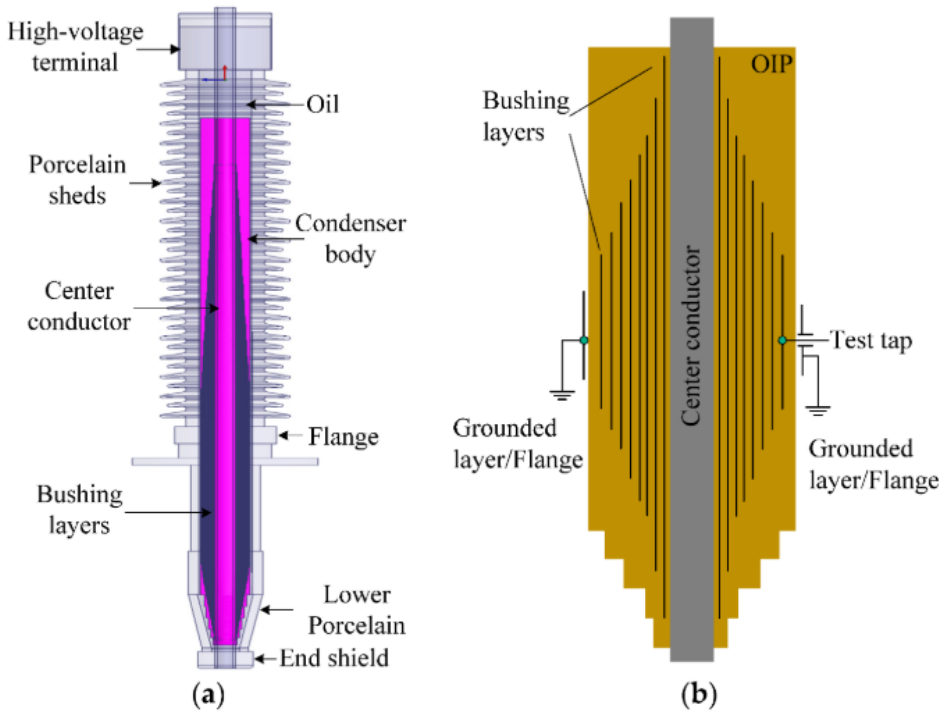


**Fig.4 Illustration of an oil-impregnated paper (OIP) bushing (not to scale)
(a) overall structure; (b) the condenser bushing body [12].**

Paper and aluminium foil are wrapped around the hollow central conductor of the type. The centre conductor carries the paper insulation layers and condenser layers wound on it [4].

The space between the centre conductor and the insulation paper and condenser layers is filled with insulation oil. This oil is used both for insulation and to prevent moisture. This oil has no contact with the oil in the transformer boiler [4].

The electric field of the centre conductor decreases as it goes out of the condenser layers, it is not homogeneously distributed to all condenser layers. In order for the electric field to be homogeneous, the width and length of the cylindrical condenser layers must be in a certain ratio. Thanks to this design, the condenser layers provide homogeneous electric field and induction voltage distribution on the insulation between the centre conductor and the grounded flange [4].

The condenser is designed so that the capacity values of the floors are equal. The capacity value is directly proportional to the length of the layers and inversely

proportional to the natural logarithmic value of the radius ratio of the layers with respect to the centre conductor. Therefore, the surface areas of the layers affect the capacity value. The width of the aluminium layers increases as the winding thickens as you go outwards. As you move outwards to equalise the surface area, the aluminium layer lengths become shorter. Thus, the capacity values of the condenser floors are approximately equalised [4].

The condenser layers prevent direct discharge into the tank by dividing the phase-ground induction voltage generated by the centre conductor into equal parts by the number of layers. The divided induction voltage is transmitted to the ground at zero potential through the top end. Each condenser layer divides the induction voltage and reduces it to zero value at the last condenser layer [4].

If the tep cover remains open during operation, the induction voltages generated in the condenser layers have difficulty in discharging since the tep and tep layers cannot provide ground contact. In this case, it may cause heating in the tep region and may cause deterioration of the insulation of the tep and condenser layers [4].

The supporting flange is used both to connect the bushing with the transformer tank and to transmit capacitive voltages accumulated in the condenser layers and transmitted to the flange through the top to the earthed tank. The earth connection of the flange is made through the transformer tank. If the earth contact of the flange is not provided, the capacitive voltages formed on the condenser layers cannot be transmitted to the earth. This may cause heating in the bushing, insulation deterioration and bushing explosion [4].

The oil level indicator monitors the level of insulating oil filling the area between the centre conductor and the outer porcelain. This level should not fall below certain levels for summer and winter months. In summer, the oil expands and the trapped oil may damage the bushing. This should be taken into consideration. If the oil level drops, the cause must be investigated and measures must be taken. Because a decrease in the insulation oil level in the bushings may cause serious damage. If the oil level indicator shows a change in the colour of the insulating oil or if the colour of the insulating oil is different from the others, this may indicate a malfunction [4].



Fig.5 OIP Bushing.

Resin-Impregnated Bushings (RIP)

Crepe paper is wrapped over a conductor to form a solid insulation. Conductor inserts made of aluminium are placed axially and radially to create uniform electric field. The core is heated and vacuum dried and then impregnated using curable epoxy resin to form the condenser core. The flange and insulator are then fitted [13].

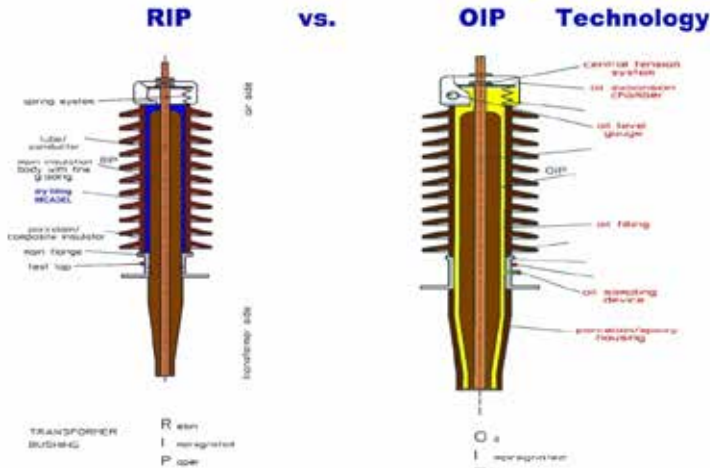


Fig.6 RIP and OIP Bushing [14].

If we compare epoxy impregnated and resin impregnated insulation materials, epoxy impregnated paper has lower thermal conductivity. If the temperature of the epoxy impregnated insulating paper is too high, the coefficient of thermal expansion of the core also increases, which can lead to thermal stress. Thermal stress leads to cracking of the core and insulation failures in epoxy impregnated paper. According to researches, most of the transformer failures are caused by the expansion of RIP bushings due to high temperature. As the current carried increases, the epoxy impregnated insulating paper in the RIP bushings may not be able to withstand the heat. Therefore, the design of RIP bushings is difficult [15].

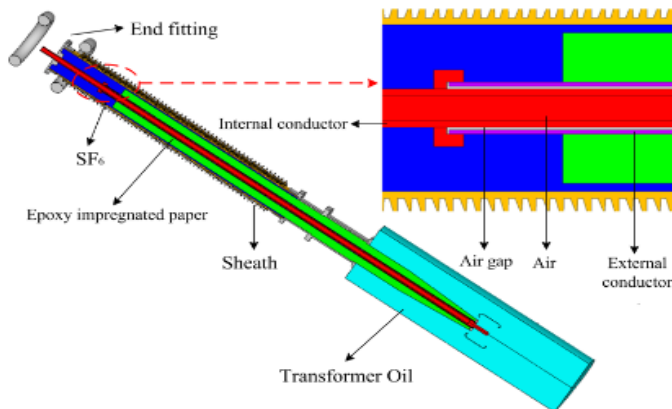


Figure 1. 3D model of the 400 kV converter transformer bushing.

Fig.7 3D Model of the 400 kV Converter Transformer Bushing [15].

It is the simulation model of the 400 kV RIP bushing modelled above. Transformer RIP bushing consist of SF6 (Sulfur Hexafluoride) gas, epoxy impregnated paper, sheath, transformer oil, internal conductor, external conductor and air gap as shown above. The internal conductor is made of copper. Therefore it has high thermal conductivity. The external conductor is equipotential with the internal conductor, but does not participate in current carrying, it is made of aluminium alloy [15].

The advantages of RIP bushings are following:

- It is earthquake resistant due to its high mechanical strength, flexibility and light weight.

- Since there is no oil in the bushing, there is no need to have an expansion volume at its highest point. This requires that they can be energised immediately after installation, even if the RIP bushings are stored horizontally.

- If the bushing explosion, it eliminates the risk of oil spilling into the equipment and causing a fire.

- The transformer is gasketed, which means that the risk of humidity entering the transformer in case of flashover is reduced.

- Since there are no porcelain parts inside the transformer, the downtime is also reduced in case of major transformer failures [13].

According to the insulating medium at the ends of the bushing:

- air to oil bushing
- air to SF6 bushing
- air to air bushing
- oil to oil bushing
- SF6 to oil bushing [16]

Air To Oil Bushing

In such bushings, one end is produced with air insulation and one end with oil insulation. It has strong dielectric behaviour. For this reason, oil is twice as strong as air at atmospheric pressure. It is usually used between atmospheric air and an oil-filled apparatus [16].

Air To Air Bushing

In this type of bushings, both ends are air insulated. Generally, this type of

application is used in building applications where one of the ends is indoors and the other is outdoors [16].

SF6 To Oil Bushing

This type of bushing consists of two compartments. The lower compartment remains inside the transformer. The upper compartment is fixed to the transformer casing. It is used as a transition between SF6 busbar ducts and oil-filled apparatus. SF6 gas is generally used as insulation medium in high and very high voltages. SF6 gas is used because it is not subject to ageing, is non-flammable, has dielectric properties 3 times greater than air and nitrogen and has arc cutting properties [17,18].

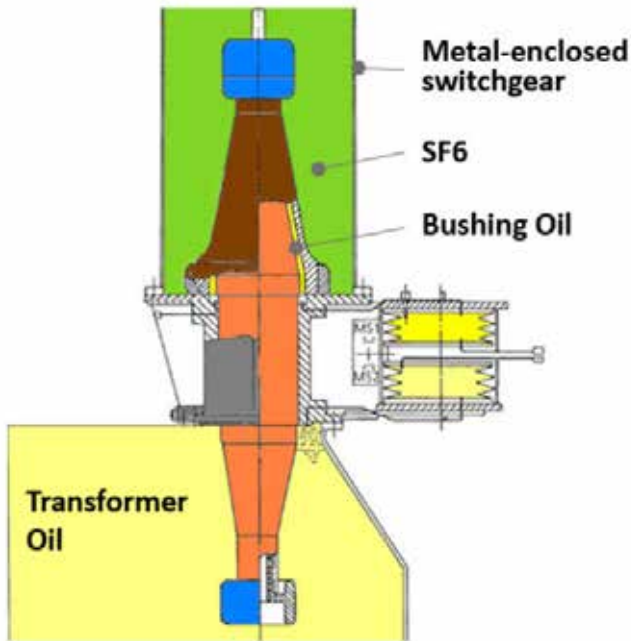


Fig.8 SF6 to oil bushing [18].

Air To SF6 Bushing

This type of bushings are mostly used in SF6 insulated circuit breakers [16].

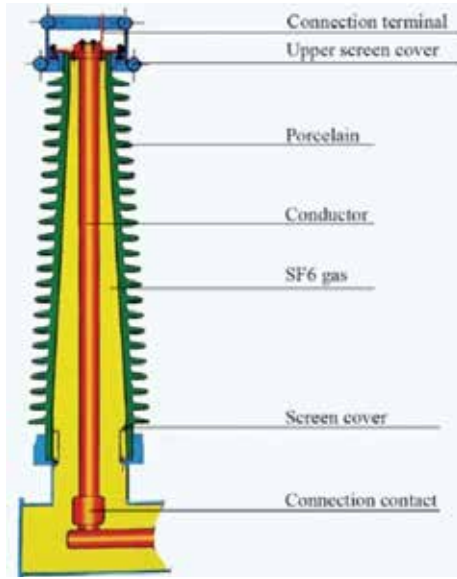


Fig.9 Air to SF6 Bushing [19].

Oil To Oil Bushing

Used between oil-filled apparatus and oil-filled bus ducts [16].



Fig.10 Oil to oil Bushing [20].

Bushing Faults in Transformers

Fouling of the surface of the bushing or fouling jumping may occur due to moisture. Fouling jumping is particularly common in transformers operating in dust-intensive areas. For this reason, it is important not to interrupt the maintenance of transformers [4].

In superficial discharges, very little damage to the bushings occurs. In porcelain bushings, melting spots can be seen on the flange as a result of discharge [4].

Bushing failures are usually caused by gaskets that prevent oil leakage and moisture. In the condenser bushings, it may be caused by deterioration of the ‘O’ ring gaskets or perforation of the condenser coats if the oil level drops [4].

CONCLUSION

In this study, the importance of bushings, the structure of bushings and bushing types are explained. Bushings are insulation elements that provide energy transmission in power transformers. The bushing failures is one of the common failures in transformer failures. They are transformer elements that must be checked in every periodic maintenance. Bushings are divided into three as dry, oily and condenser type. The most frequently encountered types are oil type bushings used in distribution transformers. Condenser type bushings are used in very high power transformers. The most commonly used type of condenser type bushings is OIP bushing. This is because the oil is the expansion reservoir.

REFERENCES

- [1] A. K. Mehta, R. N. Sharma, S. Chauhan and S. D. Agnihotri, “Study and diagnosis of the power transformer bushing insulation system,” 2011 IEEE Pulsed Power Conference, Chicago, IL, USA, 2011, pp. 700-705, doi: 10.1109/PPC.2011.6191566.
- [2] K. Li et al., “Rapid Position Determination Method for Internal Faults in Power Transformer Bushing,” 2023 International Conference on Advances in Electrical Engineering and Computer Applications (AEECA), Dalian, China, 2023, pp. 310-315, doi: 10.1109/AEECA59734.2023.00063.
- [3] O. C. Usta, “Yağ Emdirilmiş Kağıtlı Kondenser (YEKK) Buşingler İçin Farklı

- Frekanslarda Kayıp Faktörü Ölçümü”, EMO Bilimsel Dergi, Vol. 9, no. 1, pp. 37–44, 2019.
- [4] M. Pustu, “Güç Transformatörleri Ve Saha Testleri,” TMMOB Elektrik Mühendisliği Odası, Ankara, pp. 75 133-147, 2016.
- [5] J. C. Olivares-Galvan, S. Magdaleno-Adame, E. Campero-Littlewood, P. S. Georgilakis, “Techno-Economic Evaluation Of Reduction Of Low-Voltage Bushings Diameter In Single-Phase Distribution Transformers ,” 2011 Electric Power Components and Systems, Vol. 39, pp. 1388, doi:10.1080/15325008.2011.584109.
- [6] Savree, Oil-Filled Porcelain Bushing. [Online] Available At: <<https://Savree.Com/En/Encyclopedia/Oil-Filled-Porcelain-Bushing>> [Accessed 25 October 2024].
- [7] “Transformer Bushings OIP Condenser Type Up To 420 kV”, 2012 (TELK) Transformers and Electricals Kerala Limited, Kerala State, India, no. T94-007D, pp. 1.
- [8] Electricalstandards, Types Of Bushings And Voltage Ratings, 2024. [Online] Available At: <<http://Electrialstandards.Blogspot.Com/2018/04/Types-Of-Bushings-And-Voltage-Ratings.html>> [Accessed 25 October 2024].
- [9] L. Jonsson and M. Lundborg, “Dry transformer bushings with composite insulators — The obvious combination for increased reliability,” 2014 IEEE Central America and Panama Convention (CONCAPAN XXXIV), Panama, Panama, 2014, pp. 1-6, doi: 10.1109/CONCAPAN.2014.7000453.
- [10] L. Jonsson, R. Johansson, “High Voltage Bushings: 100 Years Of Technical Advancement,” ABB Review 3/2009, Ludvika, Sweden, pp. 66-70.
- [11] E. A. Feilat, I. A. Metwally, S. Al-Matri, A. S. Al-Abri, “Analysis Of The Root Causes Of Transformer Bushing Failures,” International Journal of Computer, Electrical, Automation, Control and Information Engineering, Vol. 7, No. 6, pp. 791-796, 2013.
- [12] F. Yang, L. Du, L. Yang, C. Wei, Y. Wang, L. Ran, P. He, “A Parameterization Approach For The Dielectric Response Model Of Oil Paper Insulation Using FDS Measurements,” 2018 Energies, China, 2018, 11(3), 622, doi: <https://doi.org/10.3390/en11030622>.
- [13] “Bushings for Power Transformers Product Guide,” 2014 ABB AB Components, Ludvika, Sweden, 2014, 1ZSC000653-ABF, pp. 2-8.
- [14] Micafil Rip Technology. Z. Zic 09/2003. [Online] Available At: <<https://www.>

- Scridb.Com/Document/76817815/Rip-Technology> [Accessed 25 October 2024].
- [15] Q. Wang, X. Yang, H. Tian, P. Liu and Z. Peng, “A novel dissipating heat structure of converter transformer RIP bushings based on 3-D electromagnetic-fluid-thermal analysis,” in *IEEE Transactions on Dielectrics and Electrical Insulation*, vol. 24, no. 3, pp. 1938-1946, June 2017, doi: 10.1109/TDEI.2017.006027.
- [16] Studyelectrical, *Electrical Bushings – Types, Purpose and Construction with Diagrams*, 2024. [Online] Available at: <<https://studyelectrical.com/2015/09/electrical-bushings-types-and-purpose-classification-construction.html>> [Accessed 25 October 2024].
- [17] M. N. S. Khan, “Transient Voltage Distribution In Bushing,” Degree Project In Electrical Engineering, Stockholm, Sweden, 2020, TRITA-EECS-EX-2020:939, pp. 6-13.
- [18] Seamarconi, *SF6 in Oil – Bushing Seal Defects*, 2024. [Online] Available at: <<https://www.seamarconi.com/en/critical-issues/sf6-in-oil-bushing-seal-defects/sf6-in-oil-seal-defects-bushing/>> [Accessed 25 October 2024].
- [19] Slideplayer, All Rights Reserved *Gas-Insulated Switchgear (GIS) - Ppt Download*. [Online] Available at: <<https://slideplayer.com/slide/7538753/>> [Accessed 25 October 2024].
- [20] Yash Highvoltage, *Oil To Oil Bushings*. [Online] Available at: <<https://yashhv.com/pro-oip-wall-bushings-oil-bushings>> [Accessed 25 October 2024].

CHAPTER 5

MEASUREMENT OF INSULATION PERFORMANCE OF TRANSFORMER DIELECTRIC LIQUIDS BY HARMONIC CURRENT ANALYSIS

Res. Asst. Dr. Fatih ATALAR

Istanbul University-Cerrahpaşa

Department of Electrical and Electronics Engineering

Orcid No: 0000-0002-0179-3108

Prof. Dr. Aysel ERSOY

Istanbul University-Cerrahpaşa

Department of Electrical and Electronics Engineering

Orcid No: 0000-0003-1164-7187

1. POWER TRANSFORMERS

Power transformers are indispensable components of modern energy systems and play a key role in the transmission and distribution of electrical energy (Küchler, 2017). Efficiently transporting electrical energy over long distances typically requires transmission at high voltage levels (Tan et al., 2018). Power transformers convert these voltage levels to suitable ranges for their applications (Winders, 2002), minimizing energy losses. The transformer oils used in power transformers (see Figure 1) support safe and long-lasting operation through their functions of electrical insulation and thermal management. These special oils effectively dissipate heat generated in the transformer's windings and core, preventing overheating. Additionally, their high dielectric strength improves

electrical insulation and helps protect the transformer against risks such as short circuits or arcing.

The performance of transformer oils directly impacts the operational efficiency and lifespan of the transformer. Over time, transformer oil can be exposed to environmental factors such as oxidation, moisture absorption, and contamination. This exposure can reduce the oil's dielectric strength, adversely affecting its insulation and cooling performance. In particular, acidic compounds formed due to oxidation can lead to corrosion within the transformer and weaken insulating materials. Therefore, regular analysis and maintenance of transformer oils are crucial for monitoring quality parameters and ensuring the safety of the transformer (Thiviyathan et al., 2022).

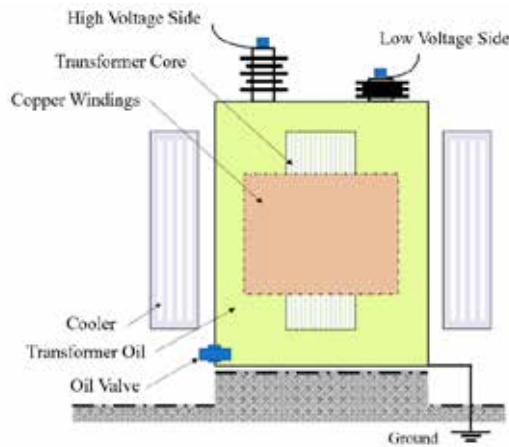


Figure 1. Power Transformer and Dielectric Liquid (Benmahamed, 2021)

When using transformer oils, environmental and safety factors must also be considered. Traditional mineral-based transformer oils pose environmental risks; therefore, biodegradable and non-toxic alternative oils, such as natural esters, are gaining increasing importance. Additionally, to mitigate safety risks like transformer fires, oils with high flash points and low flammability characteristics are preferred. Compliance with environmental regulations and sustainability goals plays a critical role in the energy sector's ability to fulfill both its economic and ethical responsibilities (Jin et al., 2022). Transitioning to safer and more environmentally friendly insulating liquids not only enhances operational safety but also aligns with global efforts toward reducing ecological impact and promoting sustainable practices in energy production and distribution.

1.1. Mineral Oils

Mineral oils are hydrocarbon-based insulating liquids obtained through the distillation and refining of crude oil (Grob, 2018). The mineral oils used in transformers are generally categorized into two main types:

Paraffin-Based Mineral Oils: These oils contain high molecular weight hydrocarbons and exhibit good oxidation stability. However, they tend to crystallize at low temperatures, which can reduce their liquidity.

Naphthenic-Based Mineral Oils: These oils have a lower molecular weight and demonstrate better liquidity at low temperatures. They also produce less sludge during oxidation, providing advantages for long-term use.

In terms of heat transfer, mineral oils dissipate heat from hot spots within the transformer through natural convection and conduction mechanisms (Soni & Mehta, 2023). The thermal conductivity equation can be expressed in equation 1.

$$q = k \cdot \frac{dT}{dx} \quad (1)$$

In this context, q represents the heat flux per unit area (W/m^2), k is the thermal conductivity of the mineral oil ($\text{W}/\text{m}\cdot\text{K}$), and $\frac{dT}{dx}$ is the temperature gradient. The thermal conductivity of mineral oils typically ranges from 0.1 to 0.15 $\text{W}/\text{m}\cdot\text{K}$.

From an electrical insulation perspective, mineral oils can withstand electric field strength and fulfill their insulation function. The electric field influences the insulation capacity of the oil in the equation 2.

$$E = \frac{V}{d} \quad (2)$$

In this equation, E represents the electric field strength (V/m), V is the applied voltage (V), and d is the thickness of the oil (mm). The dielectric strength of mineral oils typically ranges from 30 to 50 kV/mm (Kiran et al., 2022). Mineral oils are prone to sludge formation during oxidation, which can damage the electrical insulation papers and metal components inside the transformer. Additionally, mineral oils carry a fire risk; their flash points generally fall within the range of 130°C to 150°C .

1.2. Ester Liquids

Ester liquids are special liquids used for insulation and cooling purposes in electrical transformers and high voltage applications. These liquids are generally obtained by chemically esterifying vegetable oils. The chemical structure of ester liquids consists of ester groups formed by the reaction of saturated and unsaturated fatty acids with alcohol. Its general formula is expressed as RCOOR', where R is defined as the alkyl group, while R' represents the alcohol radical. The physical properties of these liquids include low viscosity, high dielectric strength and good thermal conductivity (Rao et al., 2020). While low viscosity increases the cooling performance of ester liquids, high dielectric strength can generally reach 30 kV/mm or more. Ester liquids also attract attention with their environmentally friendly properties, being easily biodegradable and thus minimising environmental impacts (Farade et al., 2023). They are also more advantageous than mineral oils in terms of fire safety, as they reduce environmental impacts and increase safety when used in areas with a fire risk. It is notable that certain ester liquids exhibit reduced flammability in Class K fire classification, underscoring their potential for application in high-risk environments. The versatility of ester liquids is evident in their wide range of uses, including insulation and cooling in electrical transformers, reliability in high-voltage equipment, and as environmentally friendly alternatives in renewable energy systems. A distinguishing feature of ester liquids is their polar structure, which contributes to their electrical insulation performance. The polar molecules in ester liquids help protect insulation papers from moisture by binding water molecules, thereby delaying the deterioration of insulation papers and extending transformer life (Rozga et al., 2020).

In relation to the transfer of heat, ester liquids are distinguished by their low viscosity and high thermal capacity. These liquids have the capacity to effectively cool the transformer's hot spots. The Nusselt number is utilised to assess the performance of heat transfer as shown in equation 3.

$$Nu = \frac{h.L}{k} \tag{3}$$

where, Nu is the Nusselt number, h is the heat transfer coefficient, the L is characteristic length and the k is thermal conductivity (Wang et al., 2023). It is demonstrated that the thermal capacity cp of ester liquids can exceed that of mineral oils, enabling superior absorption of temperature fluctuations. In terms

of fire safety, ester liquids are significantly superior to mineral oils, with a flash point typically exceeding 300°C. This characteristic renders them particularly well-suited for applications in fire-prone areas. Additionally, ester liquids exhibit a high degree of biodegradability, reaching up to 95%, thereby minimising their environmental impact. The superior performance characteristics of ester liquids, including their high insulation performance and temperature tolerance, make them a clear choice over mineral oils. Their higher dielectric strength contributes to their enhanced insulation performance, while their temperature tolerance ensures stability across a broad range of conditions. However, it should be noted that ester liquids generally incur a higher financial outlay than mineral oils; nevertheless, their long-term advantages can lead to a reduction in maintenance and repair costs. In applications where safety is of paramount importance, the cost-effectiveness of ester liquids becomes more evident.

2. HARMONIC CURRENT ANALYSIS

Harmonics are defined as multiples of the fundamental frequency of voltage and current waves. For instance, if a system has a fundamental frequency of 50 Hz, frequencies such as 100 Hz and 150 Hz are termed second and third harmonics, respectively. These harmonic components have the capacity to affect the total current and voltage waveforms in the system, resulting in power losses and equipment failures. Consequently, harmonic current analysis is a critical process for optimising the performance of power systems. The Fourier transform is a widely used method for harmonic current analysis, as it allows a waveform to be separated into its harmonic components. This analysis is important for identifying harmonic current sources and evaluating the effects of these sources on the system. The equivalent of the time-varying $f(t)$ signal on the frequency axis (equation 4) is calculated as in Equation 4 in its simplest form (Fang et al., 2021).

$$F(w) = \int_{-\infty}^{+\infty} f(t)e^{-j\omega t} dt \quad (4)$$

A current signal has continuous sinusoidal waveform. However, in order to perform harmonic analysis, the values in each frequency band must be created separately. Therefore, the calculation method is used in equation 5 to convert samples in the time axis to samples in the frequency band (Salem et al., 2020).

$$F(k\Delta\Omega) = \sum f(n\Delta T)e^{-j2\pi kn/N} \quad (5)$$

In this equation, n increase from 0 to N-1. N is expressed as the total number of samples. $\Delta\Omega$ represents the variation of the time axis in response to frequency. For the calculation of harmonic components, the discrete transform should be continued with the fast Fourier transform. For this, calculation is made by using the equation $W = e^{j2\pi kn/N}$ in which k and n sample numbers are calculated in matrix form W_{kn} . After this stage, the harmonic values that distort the waveform are calculated using the formula in equation 6 (Yu et al., 2023).

$$i(t) = \sum_{n=1}^{\infty} i_n(t) = \sum_{n=1}^{\infty} \sqrt{2}I_n \sin(n\omega_1 t + \delta_n) \quad (6)$$

The current components that do not have a specific frequency (DC) are neglected in this equation. It shows the instantaneous value of the n^{th} degree harmonic current in the time axis. The harmonic current value at n^{th} degrees at angular frequency ω_1 and phase angle δ_n is calculated as the effective value. After that, the equation $HD_n = \frac{I_n}{I_1}$ is used to calculate each harmonic value.

Harmonic current analysis is also subject to normative requirements. Standards such as IEC 61000-4-7 (Dalali et al., 2015) and IEEE 519 provide specific criteria for measuring and evaluating harmonics (Abdalla et al., 2022). These standards help to protect power quality by defining limits for harmonic levels. It is therefore incumbent upon system engineers and designers to perform analyses in accordance with these standards.

The fifth and seventh harmonics are significant harmonic components that are frequently observed in electrical systems. The fifth harmonic occurs at a frequency five times the fundamental frequency and is typically 250 Hz (for a fundamental frequency of 50 Hz). The seventh harmonic occurs at a frequency seven times the fundamental frequency and is defined as 350 Hz. The general equation for the fifth harmonic is as follows in equation 7.

$$I_5 = I_1 \cdot \sin(5\omega t + \phi_5) \quad (7)$$

In this equation I_5 , denotes the fifth harmonic current component I_1 , represents the fundamental current, ω signifies the angular frequency ($2\pi f$), t denotes the time, and ϕ_5 represents the fifth harmonic phase angle. The equation for the

seventh harmonic is in equation 8.

$$I_7 = I_1 \cdot \sin(7\omega t + \phi_7) \quad (8)$$

In this equation I_7 , denotes the seventh harmonic current component ϕ_7 , represents the seventh harmonic phase angle.

In particular, the fifth harmonic has been shown to cause phase imbalances and torque fluctuations in motors (Yu et al., 2023). The seventh harmonic has been shown to cause increased heating of motors and other equipment. This can result in a reduction in the lifespan of the equipment and an increase in the costs of maintenance.

3. HIGH VOLTAGE TEST SETUP

To investigate the impact of dominant harmonic current on the dielectric strength of transformer oil, an advanced high AC voltage experimental setup was established utilizing various electrode configurations. This was accomplished through the application of disc and VDE-type electrodes, adhering to ASTM D1816-12 (ASTM, 2019b) and ASTM D877/87M-19 (ASTM, 2019a) standards, with a specified electrode separation of 1 mm. Initial experiments were conducted using pristine and clean oil devoid of nanoparticles. Subsequently, the oils underwent testing following the incorporation of the pertinent metals. In these experiments, commercial mineral oil, natural ester, and synthetic ester were employed. The electrical and physical characteristic values of the liquids are presented in Table 1. Both types of electrodes, constructed from brass, were utilized in accordance with the aforementioned standards. The disc component of the electrode features a diameter of 36 millimeters and a thickness of 1 centimeter. Supporting rods, measuring 8 mm in diameter and 4 cm in length, are affixed at the center of the disc. The curvature initiating the formation of the cap or mushroom point of the VDE electrode has a radius of 4 mm. The vertical dimension of the mushroom head is 36 mm in diameter, with the distance from the rearmost point to the apex of the head measuring 13 mm.

Table 1. Electrical and Physical Parameters of Dielectric Liquids

Parameter / unit	Liquid type		
	Mineral oil	Natural ester	Synthetic ester
Electrical permittivity	2.2	3.1	3.2
Dielectric dissipation factor at 90 °C	0.001	0.027	0.007
Viscosity at 40 °C [mm ² /s]	9.5	37	28
Density at 20 °C [g/cm ³]	0.87	0.92	0.97
Flash Point [°C]	150	350	260
Pour Point [°C]	-51	-31	-60
Moisture content [ppm]	6.8	56	69

A voltage transformer rated at 1.5 kVA, with a turn ratio of 220 V/32 kV, is employed to generate elevated voltage levels. This transformer is powered by an autotransformer, which allows for variable adjustment of the voltage derived from the low-voltage network. To facilitate the high voltage output of the transformer, a pre-resistor with a resistance of 1 MΩ is integrated into the system. The test vessel is constructed from plexiglass and is designed with dimensions of 15 cm x 15 cm x 15 cm, featuring a wall thickness of 10 mm. The configuration and layout of the experimental setup are depicted in Figure 2a, while the corresponding circuit schematic is illustrated in Figure 2b. This arrangement facilitates systematic experimentation, enabling detailed analysis of dielectric properties under controlled conditions.

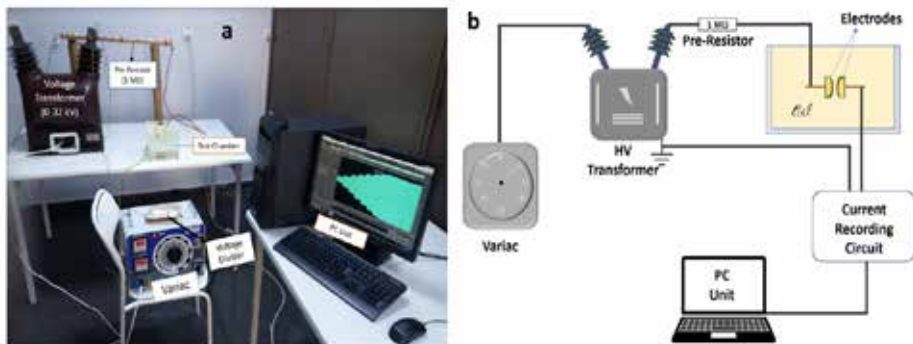


Figure 2. a: Experimental Setup b: Schematic Diagram (Atalar, 2022)

To facilitate straightforward calculations of leakage current, a voltage divider circuit was implemented, connected downstream of the ground electrode. The

voltage drop across the circuit was measured and subsequently divided by the resistance value to determine the electric current flowing through that segment of the circuit. These current values were captured in real-time by interfacing with a computer unit, utilizing a sampling frequency of 44.1 kHz for accurate data acquisition. For each experimental scenario, the tests were conducted in quintuplicate, adhering to the established standards to ensure reliability and reproducibility of the results. This systematic approach allowed for comprehensive analysis and verification of the leakage current behavior under varying conditions. Copper oxide and iron oxide nanoparticles were employed due to the oxide characteristics of metal particles that detach from conductors within transformers. The dielectric properties of the oils were assessed by incorporating 50-100 nanometer (nm) Fe_3O_4 nanoparticles at a concentration of 0.001 g/l, as well as 100 nm CuO particles at a concentration of 0.1 g/l. These nanoparticles were uniformly dispersed in the oil using a basic mechanical mixer to ensure homogeneity. The weights of the nanoparticles were precisely measured utilizing a high-accuracy scale, allowing for meticulous control over the experimental conditions. This methodology enabled a thorough investigation of how the addition of these metal oxide nanoparticles influences the dielectric behavior of transformer oils, providing valuable insights into their performance under electrical stress.

4. RESULTS

In the scope of experiments, mineral oil, natural ester and synthetic ester liquids utilised in power transformers were subjected to testing with 1 mm VDE and disk type electrodes at voltage increments of 500 V/s and 3 kV/s, respectively. The harmonic components were calculated by applying the Fourier transform to the pre-electrical breakdown part of the AC leakage current signals, which were collected with a sampling frequency of 44.1 kHz. This application was also applied to dielectric liquids with iron oxide and copper oxide additives. Single harmonic values for all test cases of the first mineral oil are given in Table 2.

Table 2. Mineral Oil Harmonic Current Values

Frequency [Hz]	Harmonic Current Values [mA]					
	Disc Electrode Arrangement			VDE Electrode Arrangement		
	Pure Mineral Oil	CuO Additive	CuO+Fe ₃ O ₄ Additive	Pure Mineral Oil	CuO Additive	CuO+Fe ₃ O ₄ Additive
50	2.72	2.24	3.26	33.56	3.04	2.82
150	0.03	0.03	0.04	0.16	0.08	0.03
250	0.12	0.03	0.02	0.51	0.06	0.03
350	0.23	0.18	0.24	1.92	0.26	0.23
450	0.15	0.13	0.17	1.97	0.14	0.15
550	0.20	0.11	0.11	1.46	0.13	0.14
650	0.15	0.11	0.15	1.35	0.10	0.13

The breakdown voltage of mineral oil, devoid of any metal particles, was measured at 4.83 kV with the disc electrode configuration and 18.48 kV with the VDE electrode configuration. Upon the introduction of copper particles, the breakdown voltage decreased to 3.6 kV at the disc electrode and 4.65 kV at the VDE electrode. Notably, after adding ferrous metal oxides to the oil, the breakdown voltage increased to 4.97 kV for the disc electrode arrangement and 6.77 kV for the VDE configuration.

As detailed in Table 2, the dominant harmonic values in untreated mineral oil at the disc electrode arrangement were the 7th and 11th harmonics. However, the addition of copper particles shifted this dominance, introducing the 13th harmonic as the prevailing component. Table 3 presents the harmonic values for natural ester liquid at both electrode configurations with a 1 mm gap.

The pure natural ester liquid exhibited total discharge at breakdown voltages of 7.68 kV and 18.96 kV for the disc and VDE electrode configurations, respectively. Following the incorporation of copper powder, breakdown voltages were recorded at 6.04 kV for the disc electrode and 14.29 kV for the VDE electrode. In the pure natural ester liquid, the 5th and 13th harmonics were more pronounced in the disc electrode arrangement, while the 11th harmonic dominated in the VDE configuration. Conversely, with the addition of copper metal particles, the 11th and 13th harmonics became dominant in the disc electrode setup, whereas the 5th and 11th harmonics were more actively represented in the VDE arrangement.

Table 3. Natural Ester Harmonic Current Values

Frequency [Hz]	Harmonic Current Values [mA]					
	Disc Electrode Arrangement			VDE Electrode Arrangement		
	Pure Natural Ester Liquid	CuO Additive	CuO+Fe ₃ O ₄ Additive	Pure Natural Ester Liquid	CuO Additive	CuO+Fe ₃ O ₄ Additive
50	9.78	7.47	7.03	29.88	14.68	11.12
150	0.15	0.04	0.04	0.19	0.06	0.24
250	1.06	0.34	0.29	1.38	1.09	0.98
350	0.68	0.45	0.44	1.41	0.64	0.53
450	0.62	0.40	0.38	1.40	0.74	0.81
550	0.70	0.46	0.42	1.60	1.01	0.85
650	0.84	0.53	0.52	1.58	0.93	0.66

In Table 4, the harmonic values for synthetic ester liquid at both electrode configurations with a 1 mm electrode gap are presented. The breakdown voltage of pure synthetic ester was recorded at 14.5 kV for the disc electrode arrangement and 23.04 kV for the VDE electrode arrangement. However, upon the addition of copper nanoparticles, the breakdown voltage significantly decreased to 10.66 kV at the disc electrode and 12.35 kV at the VDE electrode.

When iron particles were subsequently added to the synthetic ester already containing copper nanoparticles, the breakdown voltage further declined to 7.44 kV at the disc electrode arrangement, while it increased to 19.33 kV at the VDE configuration.

Table 4. Synthetic Ester Harmonic Current Values

Frequency [Hz]	Harmonic Current Values [mA]					
	Disc Electrode Arrangement			VDE Electrode Arrangement		
	Pure Synthetic Ester Liquid	CuO Additive	CuO+Fe ₃ O ₄ Additive	Pure Synthetic Ester Liquid	CuO Additive	CuO+Fe ₃ O ₄ Additive
50	132.52	16.10	8.31	32.03	8.94	20.65
150	1.55	0.35	0.11	0.41	0.17	0.44
250	10.12	1.60	0.90	2.71	0.91	2.25

350	9.56	0.96	0.41	2.02	0.77	1.40
450	7.97	1.34	0.38	1.97	0.64	1.63
550	9.83	0.94	0.66	2.36	0.57	1.90
650	8.91	0.80	0.70	2.36	0.59	1.92

Table 4 clearly illustrates that the 5th harmonic component consistently emerges as one of the dominant harmonics in all scenarios across both electrode arrangements when measuring leakage currents in synthetic ester liquid. This finding parallels observations made with mineral oil, where the 7th harmonic was predominant. In the case of synthetic ester, the introduction of copper additives altered the harmonic dynamics: it diminished the dominance of the 11th harmonic in the disc electrode arrangement, allowing the 9th harmonic to become more significant. Similarly, at the VDE electrode arrangement, the 11th and 13th harmonics were suppressed, with the 7th harmonic taking precedence. Furthermore, when iron powder was added to the synthetic ester liquid, the 13th harmonic emerged as the dominant component.

5. CONCLUSION

AC voltage tests were conducted in accordance with ASTM D1816-84a and ASTM D877-87 standards, employing a 1 mm electrode gap. The findings from the experiments indicate that synthetic ester exhibited the highest breakdown voltage when subjected to AC voltage stress in both disc and VDE electrode configurations. The experimental results revealed that the presence of the dominant fifth harmonic component at a frequency of 250 Hz significantly enhances the insulation strength of the liquid dielectric material. Conversely, it was noted that the seventh harmonic at a frequency of 350 Hz predominates in liquid dielectrics characterized by low insulation resistance.

Among the tested liquids, synthetic ester oil demonstrated the greatest resilience to electric field stress, while mineral oil exhibited the lowest breakdown strength. Notably, no substantial differences were detected between mineral oil and natural ester oil in terms of dielectric performance. A breakdown voltage difference of approximately 3 kV was observed between natural ester and mineral oil specifically in the disk-type electrode configuration. In all instances involving mineral oil, the seventh harmonic was found to be dominant, whereas

the fifth harmonic prevailed in synthetic ester.

This dominance of the fifth harmonic provides critical insights into the dielectric resistance of the liquid, representing a significant contribution to the existing literature, as such findings have not been previously documented. This underscores the importance of harmonic analysis in evaluating the performance of dielectric materials under electrical stress, particularly in transformer applications.

REFERENCES

- Abdalla, O. H., Elmasry, S., El Korfolly, M. I., & Htita, I. (2022, December). Harmonic analysis of an arc furnace load based on the IEEE 519-2014 standard. In 2022 23rd International Middle East Power Systems Conference (MEPCON) (pp. 1-7). IEEE.
- ASTM Standard Test Method for Dielectric Breakdown Voltage of Insulating Liquids Using Disk Electrodes. ASTM D877/D877M-19, 2019, doi: 10.1520/D0877-87R95.
- ASTM Standard Test Method for Dielectric Breakdown Voltage of Insulating Liquids Using VDE Electrodes, ASTM D1816-12, 2019.
- Atalar, F., Ersoy, A., & Rozga, P., (2022). Investigation of Effects of Different High Voltage Types on Dielectric Strength of Insulating Liquids. *ENERGIES*, vol.15, no.21.
- Benmahamed, Y., Kherif, O., Teguar, M., Boubakeur, A., & Ghoneim, S. S. M. (2021). Accuracy Improvement of Transformer Faults Diagnostic Based on DGA Data Using SVM-BA Classifier. *Energies*, 14(10), 2970. <https://doi.org/10.3390/en14102970>.
- Dalali, M., & Jalilian, A. (2015). Indices for measurement of harmonic distortion in power systems according to IEC 61000-4-7 standard. *IET Generation, Transmission & Distribution*, 9(14), 1903-1912.
- Fang, C., Tao, Y., Wang, J., You, H., Cui, Y., & Zhou, M. (2021). Research on leakage current waveform spectrum characteristics of artificial pollution porcelain insulator. *Frontiers in Energy Research*, 9, 798048.
- Farade, R. A., Wahab, N. I. A., Mansour, D. E. A., & Soudagar, M. E. M. (2023). The Effect of Nanoadditives in Natural Ester Dielectric Liquids: A Comprehensive Review on Stability and Thermal Properties. *IEEE Transactions on Dielectrics and Electrical Insulation*, 30(4), 1478-1492.
- Grob, K. (2018). Mineral oil hydrocarbons in food: A review. *Food Additives &*

Contaminants: Part A, 35(9), 1845-1860.

- Jin, L., Kim, D., Abu-Siada, A., & Kumar, S. (2022). Oil-immersed power transformer condition monitoring methodologies: A review. *Energies*, 15(9), 3379.
- Kiran, S. R., Mariprasath, T., Basha, C. H., Murali, M., & Reddy, M. B. (2022). Thermal degrade analysis of solid insulating materials immersed in natural ester oil and mineral oil by DGA. *Materials Today: Proceedings*, 52, 315-320.
- Küchler, A. (2017). *High Voltage Engineering: Fundamentals-Technology-Applications*. Springer.
- Rao, U. M., Fofana, I., Beroual, A., Rozga, P., Pompili, M., Calcara, L., & Rapp, K. J. (2020). A review on pre-breakdown phenomena in ester liquids: Prepared by the international study group of IEEE DEIS liquid dielectrics technical committee. *IEEE Transactions on Dielectrics and Electrical Insulation*, 27(5), 1546-1560.
- Rozga, P., Beroual, A., Przybyłek, P., Jaroszewski, M., & Strzelecki, K. (2020). A review on synthetic ester liquids for transformer applications. *Energies*, 13(23), 6429.
- Salem, A. A., Abd-Rahman, R., Al-Gailani, S. A., Kamarudin, M. S., Ahmad, H., & Salam, Z. (2020). The leakage current components as a diagnostic tool to estimate contamination level on high voltage insulators. *IEEE Access*, 8, 92514-92528.
- Soni, R., & Mehta, B. (2023). A review on transformer condition monitoring with critical investigation of mineral oil and alternate dielectric liquids. *Electric Power Systems Research*, 214, 108954.
- Tan, J. D., Koh, S. P., Au, M. T., Tiong, S. K., & Ali, K. (2018). Implementation of voltage optimization for sustainable energy. *Indonesian Journal of Electrical Engineering and Computer Science*, 12(1), 341-347.
- Thiviyathan, V. A., Ker, P. J., Leong, Y. S., Abdullah, F., Ismail, A., & Jamaludin, M. Z. (2022). Power transformer insulation system: A review on the reactions, fault detection, challenges and future prospects. *Alexandria Engineering Journal*, 61(10), 7697-7713.
- Wang, F., Ouyang, L., Song, C., Yang, Z., Li, S., Xu, Y., & Li, J. (2023). Enhancing dielectric and thermal performances of synthetic-ester insulating oil via blending with natural ester. *IEEE Transactions on Dielectrics and Electrical Insulation*, 30(3), 1115-1124.
- Winders, J. (2002). *Power transformers: principles and applications*. CRC Press.
- Yu, H., Huang, J., Li, L., & Zhao, F. (2023). Deep fractional Fourier transform. *Advances in Neural Information Processing Systems*, 36, 72761-72773.

CHAPTER 6

BIO-BASED POLYURETHANES

Assoc. Prof. Dr. Gökhan ÇAYLI

Istanbul University-Cerrahpaşa

Department of Engineering Sciences

Orcid No: 0000-0002-3395-5642

Dr. Emin ÖZDEMİR

Istanbul University-Cerrahpaşa

Department of Engineering Sciences

Orcid No: 0000-0002-6517-9270

INTRODUCTION

In addition to being a form of polymer, polyurethane is a versatile substance that is utilized in a variety of different industries. Isocyanate and polyol are the two primary components that are involved in the chemical reaction that results in the formation of polyurethane molecules. The features of this material, which may be tailored to meet the requirements of a variety of applications, include the ability to become flexible, rigid, foamy, or elastic [1-3].

Polyurethanes have a structure that is both lightweight and reliable. Chemicals, heat, and impact are all things that they are resistant to. They have the ability to insulate against both heat and sound. There is the ability to modify the degree of flexibility or hardness in accordance with the requirements.

Among the many industries that make extensive use of polyurethanes are the construction industry, the industry of thermal insulation (polyurethane foam), the

industry of furniture and decoration, the industry of automobiles, the industry of footwear, and the industry of electronics and white goods. As a result of the material's adaptability, durability, and adaptability towards customization, polyurethane has emerged as a significant requirement in a variety of industries. As a result of its capacity to offer answers to a variety of issues and to deliver results that are more effective in comparison to those of other materials, polyurethane is becoming increasingly necessary.

At the moment, the majority of polyurethanes are derived from petroleum resources. Due to the environmental concerns and sustainable development, there is a growing number of research projects focusing on the development of bio-based polyurethanes, which is in line with the objectives of lowering carbon footprints and promoting environmental sustainability. In particular, the utilization of polyols derived from vegetable oil and carbon dioxide are significant advances in the development of a reduction in dependence on petroleum. This shift indicates that the future will be more sustainable, both in terms of the environment and the economy [4-5].

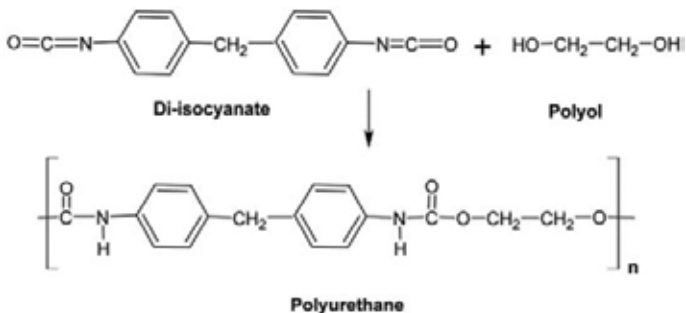


Figure 1. Structure of a typical polyurethane [6]

BIOBASED POLYURETHANES

Biobased polyurethane is a type of polyurethane that is manufactured by employing polyols that are derived from renewable biological resources rather than raw materials that are derived from petroleum reserves. It is utilized in a wide range of industrial applications, including conventional polyurethanes, but it stands out because to its low impact on the environment and decreased reliance on fossil fuels.

The use of biobased polyurethane is a significant advance in terms of its influence on the environment and its capacity to be sustainable. It is likely that in the future, biobased polyurethanes will be able to replace traditional polyurethanes. This might be made possible by increasing environmental consciousness and investments in methods that utilize renewable resources. A particular increase in the market for such products can be attributed to the efforts that are being made to reduce the carbon footprint [7-8].

When considering biobased polyurethanes, two major types of material can be counted. Those are synthesized by biobased polyols and carbonate esters of biobased epoxy compounds respectively. Although some scientist tries to develop biobased counter parts of petroleum-based isocyanates, properties of the final products are not adequate when they are compared to petroleum-based polyurethanes. The structures of the common isocyanates are shown in figure 2.

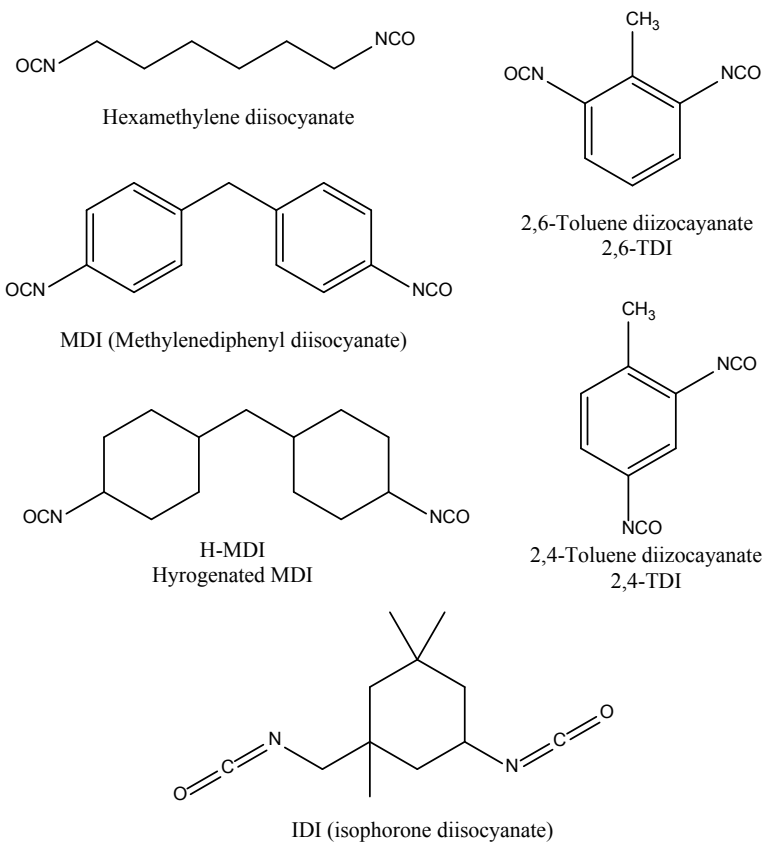


Figure 2. Structures of common isocyanates

BIOBASED POLYOLS

The manufacturing of biobased polyurethanes requires the utilization of biobased polyols, which are polymeric molecules that are generated from sustainable biological resources. Natural feedstocks, such as plant oils, sugars, lignocellulosic biomass, or proteins, are used to produce biobased polyols, in contrast to traditional polyols, which are derived from petroleum.

Polyols derived from vegetable oils are several types of biobased polyols. Produced from the triglycerides that are present in plant oils (such as soybean oil, castor oil, palm oil, canola oil, rapeseed oil, linseed oil, or sunflower oil), among other oils for example. Through the process of chemical modification, such as hydroxylation or epoxidation, the triglycerides are altered to incorporate hydroxyl groups (-OH), which renders them reactive for the purpose of polyurethane production. Take, for instance: Because it is an inherently hydroxylated oil, castor oil requires just a marginal amount of chemical treatment [9].

The first step of the synthesis of triglyceride-based polyols is the production of epoxy derivative. For this purpose, triglyceride is mixed with formic acid with hydrogen peroxide. This mixture acts as a peroxy formic acid. Reaction of peroxy acid with a double bond proceeds via concerted reaction mechanism which means all bond formation and bond breakage occur at the same time [10-12]. Reaction mechanism is shown in figure 3.

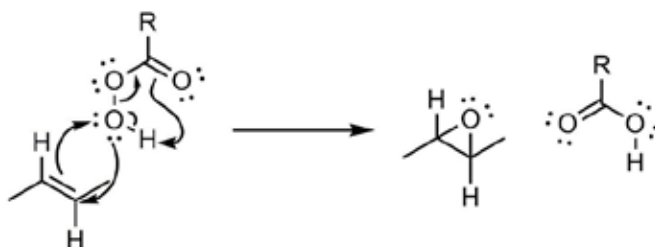


Figure 3. Reaction mechanism of epoxidation reaction

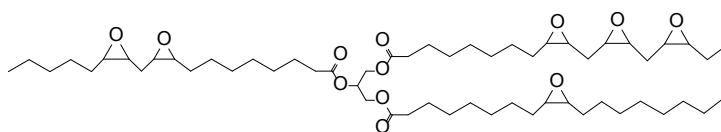


Figure 4. Structure of epoxidized plant oil triglyceride

Structure of a typical epoxidized triglyceride is shown in figure 4. Epoxy ring are strained rings and they are readily to react with electrophiles and nucleophiles. When naturally occurred carboxylic acid are reacted plant oil based epoxides, the final product is completely organic carbon containing and biodegradable material. Reactions are generally carried out between 100-130 °C. Some tertiary amines such as DABCO (1,4-Diazabicyclo[2.2.2]octane) and lewis acids such as zinc chloride, aluminum chloride and boron tri fluoride can be used as catalyst. Reactions are usually completed in 8 hours [13-15].

The Polyols Derived from Carbohydrates derived from sugars (such as glucose, fructose, and sucrose) or starch-based biomass (such as corn, potatoes, and wheat), among other sources. In order to manufacture these polyols, chemical transformations or fermentation procedures are utilized. These processes result in the production of polyols that include hydroxyl groups. Therefore, sorbitol, polyols based on sucrose, and glycerol are some examples.

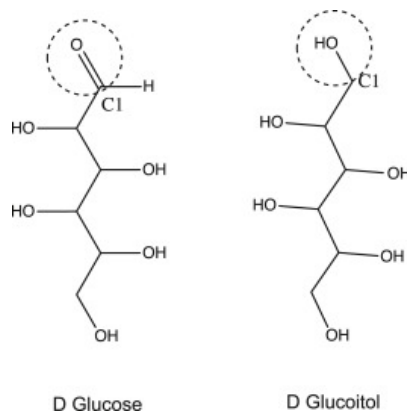


Figure 5. Polyols derived from carbohydrates [16]

In order to produce polyols that are derived from carbohydrates, a number of chemical reactions must first be carried out. These reactions transform carbohydrates into polyhydroxy molecules. The food industry, the pharmaceutical industry, and the production of polymers are just some of the businesses that make extensive use of these polyols. Main synthetic procedures can be listed as below:

1-Hydrogenation of sugars

- 2-Reduction of sugar derivatives (such as, esters and lactones)
- 3-As a reaction products of epoxies and sugars or sugar derivatives
- 4- Fermentation
- 5- Modification of carbohydrates
- 6-Dehydration (synthesis of furan derivatives)

The production of pulp and paper results in the production of lignin, which is an aromatic polymer that is found in abundance in biomass and woody plants. By converting lignin, a complex polymer that occurs naturally in the cell walls of plants, into polyhydroxy compounds, it is possible to produce polyols that are based on lignin. Polyurethanes, resins, and adhesives are all products that can benefit from the utilization of these polyols in various applications. In most cases, the synthesis begins with the depolymerization of lignin into smaller, more reactive units. Furthermore, these fragments are subjected to chemical modification in order to either introduce or enhance hydroxyl groups. Because of their rigidity, thermal stability, and low environmental footprint, polyols that are based on lignin are particularly valuable. Besides depolymerization method, hydrolysis and alkoxylation, esterification and transesterification, hydroxymethylation, phenolation, oxypropylation and blending with polyols can be used for the synthesis of lignin based polyols [17]. Oxypropylation of lignin is exhibited in figure 6.

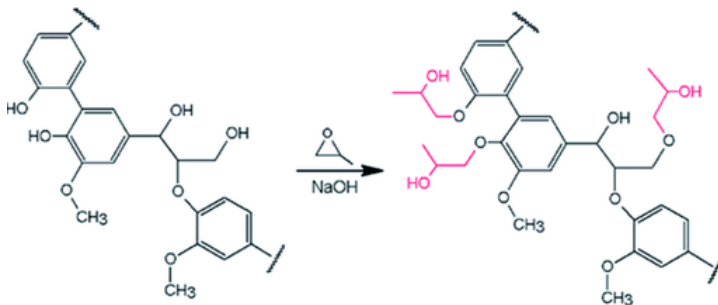


Figure 6. Schematic presentation of lignin based polyols via reaction of lignin with propylene oxide [18]

Protein-based polyols are produced by chemically altering proteins (or protein-derived peptides) in order to add numerous hydroxyl groups. This process renders the proteins appropriate for usage as polyols in applications such as the creation of polyurethane, adhesives, and other bio-based products. When

it comes to the synthesis of polyols based on proteins, the process often entails breaking down proteins into smaller units and then altering those units in order to boost their reactivity and hydroxyl functionality. Polyol synthesis by hydrolysis is depicted in figure 7. Protein based polyols can be obtained via hydrolysis of protein, amination or alkoxylation, hydroxymethylation, transesterification, esterification with polyols and fermentation methods.

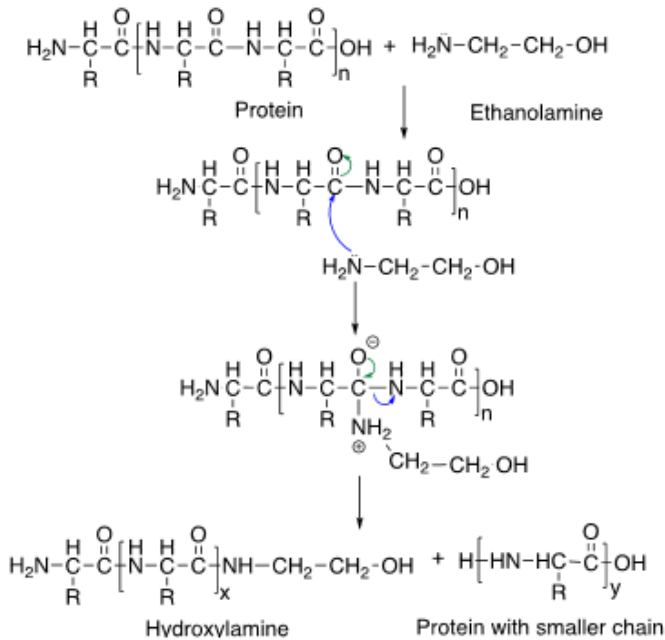


Figure 7. Synthesis of protein based polyols from Soybean Proteins via transamidation reaction. [19]

CYCLIC CARBONATES AS A BIOBASED PRECURSOR

The production of polyurethanes from cyclic carbonates is a process that is both environmentally friendly and very efficient, and it does not involve the use of isocyanates. Polyhydroxyurethanes (PHUs) are typically produced through the reaction of cyclic carbonates with amines, which is the general procedure for this synthesis.

This reaction route avoids the use of toxic isocyanates, cyclic carbonates are obtained from the reaction between carbon dioxide and plant oil based epoxides and finally that route does not require extreme reaction conditions [20].

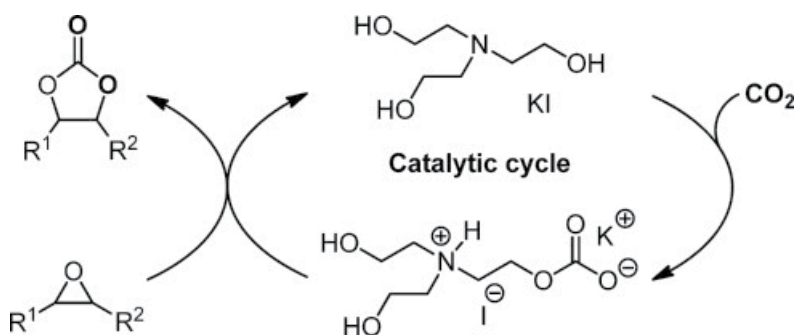


Figure 8. Synthesis of cyclic carbonates from epoxides and carbon dioxide [21]

The sequence of events that constitute the general mechanism are as follows:

1-It is possible to activate the epoxide with the use of a catalyst, such as a Lewis acid, a Lewis base, or a bifunctional catalyst. This is accomplished by increasing the electrophilicity of the epoxide.

2-Nucleophilic attack: A nucleophile, which is typically supplied by the catalyst, attacks the carbon of the epoxide that is less hindered, which results in the opening of the ring.

3- CO₂ insertion: During the CO₂ insertion process, the alkoxide intermediate that is produced has a reaction with CO₂ to produce a carbonate intermediate.

4-Ring Closure: This process results in intramolecular cyclization, which leads to the formation of cyclic carbonate.

In this process, catalysts are an extremely important component. The following are examples of common types:

-Metal complexes, such as zinc, cobalt, chromium, or aluminum complexes, are examples of homogeneous catalysts at work.

-Ammonium or phosphonium salts: Quaternary ammonium or phosphonium salts containing halide anions (for example, tetra-n-butyl ammonium bromide, also known as TBAB).

-Frameworks made of metal-organic compounds (MOFs) are heterogeneous catalysts.

-Zeolites or silica that has been functionalized.

-Metal oxides that are supported.

-In the case of bifunctional catalysts, nucleophilic and Lewis acid sites are combined. For example, metal salen complexes or ionic liquids that contain

functional groups are examples of such catalysts.

When considering reaction conditions, temperature ranges typically between 50 and 150 °C. CO₂ pressures may applied between 1-10 MPa, while there are some systems that function at atmospheric pressure by the utilization of effective catalysts. Typically, there is no need for a solvent; nevertheless, polar solvents such as acetonitrile and dichloromethane may be utilized sometimes.

BIOBASED ISOCYANATES

Almost all of isocyanates are produced from petroleum based sources. Due to their reactivity and difficulty in the synthesis, bio-based isocyanates are not common today. Because of the environmental concerns and sustainable development, In the field of isocyanate synthesis, the number of new searches continues to rise [22]

Tolonate™ X FLO 100, STABIO™ D-370N and Desmodur® eco N 7300 can be found as an industrially available biobased isocyanates. Tolanate contains 13% isocyanate functionality and 25% biomass while Desmodur and Stabio may contain 25 % isocyanate group and 70 % biomass respectively [23-25].

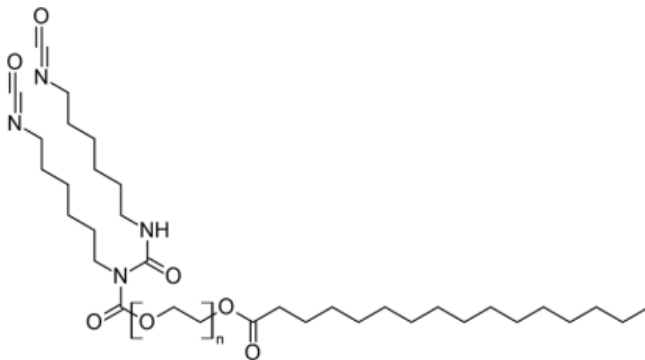


Figure 9. Structure of Tolanate X FLO 100

Kusefoğlu et al also reported biobased isocyanates from renewable resources by using AgNCO salts. The product is soft and rubbery materials and the thermal and mechanical properties of the synthesized materials are not as good as petroleum based ones [26-27].

FUTURE TRENDS

Although 100 % biobased polyurethanes is not synthesized yet, there are promising works on them. Tolanate, stabio and desmodure can be obtained in industrial scale and they contain considerable amount of biobased materials. While mechanical and thermal properties of those material expressen and discussed in the chapter, those values are noticeably close to the materials obtained from petroleum based materials. In the future, biobased polyurethanes (PU) will be driven by the growing demand for environmentally friendly materials, the regulatory pressure that is being placed on products that are derived from petroleum, and the breakthroughs that have been made in biopolymer technology. In order to produce polyols and isocyanates for biobased polyurethane, researchers are investigating a larger variety of renewable sources, such as vegetable oils (soy, castor, palm), lignin, and other agricultural leftovers. The objective of the innovations is to enhance the mechanical, thermal, and chemical capabilities of biobased polyurethanes, with the goal of making them economically competitive with their petroleum-based equivalents in applications that are particularly demanding. The incorporation of the circular economy: The development of synthetic polyurethane (PU) materials that are recyclable or biodegradable is gaining momentum, which is in line with the principles of the circular economy to reduce waste and damage to the environment. The expansion of applications involves the use of biobased polyurethanes in a variety of industries, including as the automobile industry, the construction industry, the medical device industry, and the footwear industry, all of which are progressively prioritizing the use of sustainable materials. The goal of the efforts being made to improve manufacturing processes and scale-up technologies seems to reduce the cost of biobased PU, which will therefore make it more accessible to a wider range of markets. It is believed that pressure from both regulators and consumers: The adoption of biobased polyurethanes is accelerating around the world as a result of stringent environmental rules and a growing preference among consumers for environmentally friendly products. When considering to these trends, there will be a substantial change in the next years toward polyurethane solutions that are more environmentally friendly.

REFERENCES

- 1- de Souza, F. M., Kahol, P. K., & Gupta, R. K. (n.d.). Introduction to polyurethane chemistry. *Polyurethane Chemistry: Renewable Polyols and Isocyanates*, 1–24.
- 2- Heath, D. E., Guelcher, S. A., & Cooper, S. L. (2020). Polyurethanes. In W. R. Wagner, S. E. Sakiyama-Elbert, G. Zhang, & M. J. Yaszemski (Eds.), *Biomaterials Science* (4th ed., pp. 103–107). Academic Press.
- 3- Engels, H.-W., Pirkl, H.-G., Albers, R., Albach, R. W., Krause, J., Hoffmann, A., Casselmann, H., & Dormish, J. (2013). Polyurethanes: Versatile materials and sustainable problem solvers for today's challenges. *Angewandte Chemie International Edition*, 52(36), 9422–9441.
- 4- Sonnenschein, M. F., & Koonce, W. (2011). Polyurethanes. In *Encyclopedia of Polymer Science and Technology* (Ed.).
- 5- Burke, A., Hasirci, N. (2004). Polyurethanes in biomedical applications. In N. Hasirci & V. Hasirci (Eds.), *Biomaterials* (Vol. 553, pp. 131–152). Springer.
- 6- Fazli, A., Rodrigue, D. (2020). Waste rubber recycling: A review on the evolution and properties of thermoplastic elastomers. *Materials*, 13(3), 782.
- 7- Wendels, S., & Avérous, L. (2021). Biobased polyurethanes for biomedical applications. *Bioactive Materials*, 6(4), 1083–1106.
- 8- Zhang, C., Madbouly, S. A., & Kessler, M. R. (2015). Biobased polyurethanes prepared from different vegetable oils. *ACS Applied Materials & Interfaces*, 7(2), 1226–1233.
- 9- Mutlu, H., Meier, M. A. R. (2010). Castor oil as a renewable resource for the chemical industry. *European Journal of Lipid Science and Technology*, 112(1), 10–30.
- 10- Kousaalya, A. B., Beyene, S. D., Ayalew, B., et al. (2019). Epoxidation kinetics of high-linolenic triglyceride catalyzed by solid acidic-ion exchange resin. *Scientific Reports*, 9, 8987.
11. Wang, Y., Cao, X., Shi, J., Li, X., Liu, Y., & Xu, Y.-J. (2023). Tracking the dynamics of epoxy triglycerides during thermal oxidation by liquid chromatography-mass spectrometry. *Food Control*, 146, 109523.
12. Goud, V. V., Patwardhan, A. V., & Pradhan, N. C. (2007). Kinetics of in situ epoxidation of natural unsaturated triglycerides catalyzed by acidic ion exchange resin. *Industrial & Engineering Chemistry Research*, 46(10), 3078–3085.
13. Öztürk, C., Küsefoğlu, S. H. (2010). New polymers from plant oil derivatives and styrene-maleic anhydride copolymers. *Journal of Applied Polymer Science*,

- 116(1), 355–365.
14. Wang, X., Tang, Q., Popowicz, G. M., Yang, B., & Wang, Y. (2015). A mechanistic study into the epoxidation of carboxylic acid and alkene in a mono, diacylglycerol lipase. *Biochemical and Biophysical Research Communications*, 460(2), 392–396.
 15. Scala, J. L., & Wool, R. P. (2002). The effect of fatty acid composition on the acrylation kinetics of epoxidized triacylglycerols. *Journal of the American Oil Chemists' Society*, 79(1), 59–63.
 16. Zeece, M. (2020). Flavors. In M. Zeece (Ed.), *Introduction to the Chemistry of Food* (pp. 213–250). Academic Press.
 17. Gouveia, J. R., da Costa, C. L., Tavares, L. B., & dos Santos, D. J. (2019). Synthesis of lignin-based polyurethanes: A mini-review. *Volume*, 16,(4), 345–352.
 18. Wu, M., Peng, J.-J., Dong, Y.-M., Pang, J.-H., & Zhang, X.-M. (2022). Preparation of rigid polyurethane foam from lignopolyol obtained through mild oxypropylation. *RSC Advances*, 12, 21736–21741.
 19. Bote, S. D., & Narayan, R. (2021). Synthesis of biobased polyols from soybean meal for application in rigid polyurethane foams. *Industrial & Engineering Chemistry Research*, 60(16), 5733–5743.
 20. Cokoja, M., Wilhelm, M. E., Anthofer, M. H., Herrmann, W. A., & Kühn, F. E. (2015). Synthesis of cyclic carbonates from epoxides and carbon dioxide by using organocatalysts. *ChemSusChem*, 8, (15), 2436–2454.
 21. Werner, T., Tenhumberg, N. (2014). Synthesis of cyclic carbonates from epoxides and CO₂ catalyzed by potassium iodide and amino alcohols. *Journal of CO₂ Utilization*, 7, 39–45.
 22. Niesiobędzka, J., & Datta, J. (2023). Challenges and recent advances in bio-based isocyanate production. *Green Chemistry*, 25, 2482–2496
 - 23- Vencorex, <https://www.vencorex.com/product/tolonate-xflo-100/>, 2021
 - 24- https://solutions.covestro.com/en/products/desmodur/desmodur-eco-n-7300_84603813-18871289?SelectedCountry=PL, 2019
 - 25- Mitsui Chemicals, <https://cms.ice.be/files/249/tds-stabiopresentation-.pdf>, 2021
 26. Cayli, G., Kusefoglul, S. (2008). Biobased polyisocyanates from plant oil triglycerides: Synthesis, polymerization, and characterization. *Journal of Applied Polymer Science*, 109,(5), 2948–2955.
 27. Cayli, G., Kusefoglul, S. (2010). A simple one-step synthesis and polymerization of plant oil triglyceride iodo isocyanates. *Journal of Applied Polymer Science*, 116, (4), 2433–2440. <https://doi.org/10.1002/app.31857>

CHAPTER 7

BIOBASED ANTIBACTERIAL MATERIALS

Assoc. Prof. Dr. Gökhan ÇAYLI

Istanbul University-Cerrahpaşa

Department of Engineering Sciences

Orcid No: 0000-0002-3395-5642

INTRODUCTION

Antibacterial materials are chemicals or materials that are meant to limit the growth of bacteria or kill bacteria, hence minimizing the risk of bacterial illnesses or contamination. These materials either inhibit the growth of bacteria (also known as bacteriostatic effects) or destroy bacteria (also known as bactericidal effects). Antibacterial materials have gained significant attention in recent years due to the increasing prevalence of antibiotic-resistant bacteria and the need for more effective antimicrobial solutions (Babu et al., 2013). The effects of these materials on harmful bacteria, make them valuable in a variety of applications, such as medical devices, wound dressings, and food packaging. While traditional antibacterial agents have been widely used, the search for more sustainable and environmentally friendly alternatives has led to the development of biobased antibacterial materials. (Han et al., 2020). Same examples of antibacterial agents are shown in figure 1.

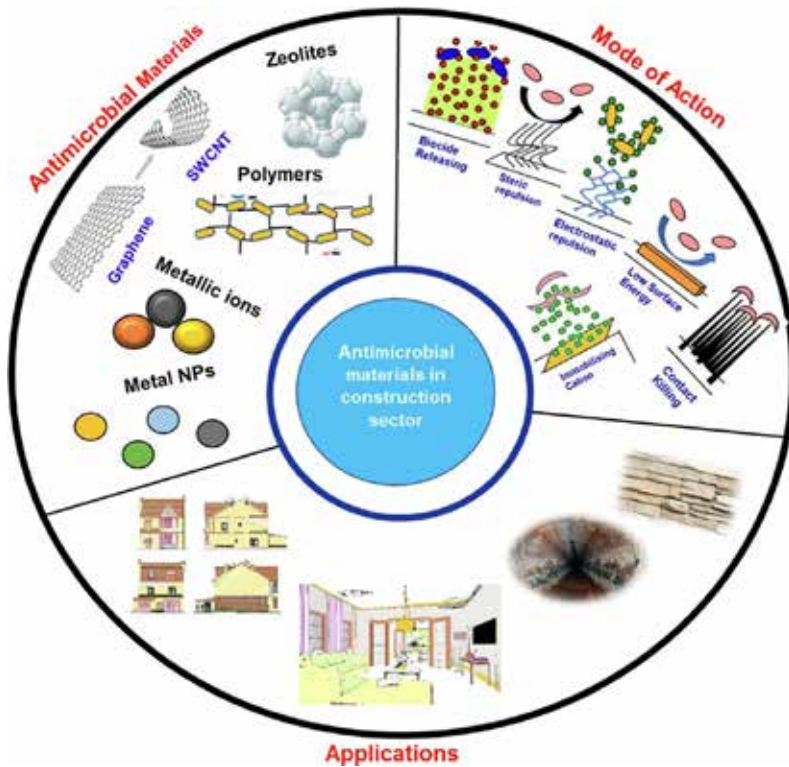


Figure 1. Same examples of Antibacterial materials (Kirthika 2023)

Biobased antibacterial materials are derived from natural sources and often exhibit inherent antimicrobial properties. These materials can be designed to target specific bacterial strains, minimize the risk of resistance development, and have a reduced environmental impact compared to synthetic antimicrobial agents. This comprehensive review will explore the definition, action mechanisms, and types of antibacterial materials, as well as the resources needed for their development.

Definition and Action Mechanisms of Antibacterial Materials

Antibacterial materials are substances that can inhibit or kill bacterial growth and proliferation. These materials can act through various mechanisms, such as disrupting the bacterial cell membrane, interfering with cellular metabolism, or preventing bacterial adhesion and biofilm formation. (Khan & Shakoor, 2023) (Agnihotri & Dhiman, 2017). The action mechanisms of antibacterial materials

can be classified into several categories:

Cell membrane disruption: Some antibacterial materials, such as certain natural antimicrobial peptides, can interact with and disrupt the bacterial cell membrane, leading to cell lysis and death which is shown in figure 2 (Khan & Shakoor, 2023).

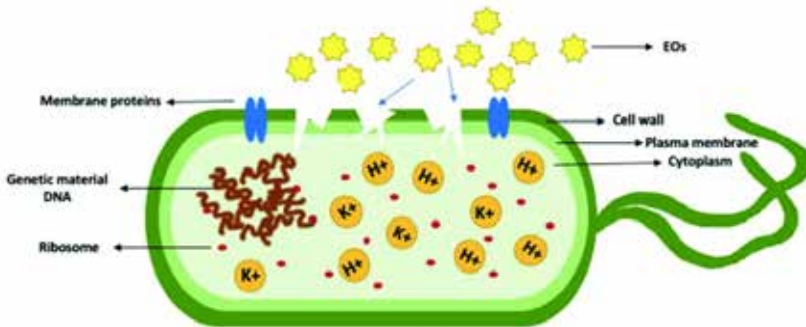


Figure 2. Schematic presentation of cell membran disruption via essential oils (Aljafaari 2021)

Interference with cellular metabolism: Other antibacterial materials may interfere with essential cellular processes, such as protein synthesis, DNA replication, or energy production, thereby inhibiting bacterial growth and survival .

Inhibition of bacterial adhesion and biofilm formation: Certain antibacterial materials can prevent the attachment of bacteria to surfaces or disrupt the formation of bacterial biofilms, which are resistant to traditional antimicrobial agents. The specific action mechanism of an antibacterial material depends on its chemical composition, physical properties, and the target bacterial strain.

TYPES OF ANTIBACTERIAL MATERIALS

Antibacterial materials can be classified into several categories based on their composition and source:

Natural Antimicrobials: These are compounds derived from natural sources, such as plants, animals, and microorganisms. Examples include phenolic compounds, terpenes, bacteriocins, peptides, enzymes, and essential oils (Fan et al., 2018). Examples are:

-Silver (Ag): Used since ancient times for wound care and water purification due to its bactericidal properties.

-Copper (Cu): Known for its ability to disrupt bacterial membranes and has been used in cookware and water vessels.

-Honey: Contains hydrogen peroxide and low pH, making it effective against bacterial infections.

-Garlic (Allicin): A natural compound with potent antibacterial effects.

-Essential Oils: Oils like tea tree, oregano, and eucalyptus have antimicrobial properties.

Synthetic Antimicrobials: These are antimicrobial agents that are chemically synthesized, often based on the structures of natural antimicrobials. Examples are:

-Antibiotics: These are drugs like penicillin, tetracycline, and erythromycin, which target bacterial infections in medical treatments.

-Quaternary Ammonium Compounds (Quats): Used in cleaning agents and disinfectants.

-Alcohols: Ethanol and isopropanol are commonly used as disinfectants.

-Chlorine and Hypochlorite: Found in bleach and used for water disinfection.

-Phenolic Compounds: Used in antiseptics like triclosan and mouthwashes.

-Peroxides: Hydrogen peroxide is a common antiseptic for wound cleaning.

Inorganic Antimicrobials: Substances that are formed of inorganic compounds or elements that display antibacterial properties are referred to as inorganic antibacterial materials. Metal ions or inorganic compounds are frequently utilized by these materials in order to either restrict the growth of

germs or kill microorganisms. They are highly regarded due to their longevity, resilience to heat, and effectiveness over an extended period of time in comparison to organic antibacterial agents. Some examples are listed below.

1. Metal-Based Antibacterial Agents

Silver (Ag): Releasing of silver ions (Ag-) that disrupt bacterial cell membranes, proteins, and DNA.

Copper (Cu): It interferes with bacterial metabolism and damages bacterial DNA.

Zinc (Zn): Zinc ions interfere with bacterial enzyme systems.

Gold (Au): Gold nanoparticles generate reactive oxygen species that damage bacteria.

2. Metal Oxides

Zinc Oxide (ZnO): They generate reactive oxygen species (ROS) and disrupts bacterial membranes.

Titanium Dioxide (TiO₂): They act as a photocatalyst under UV light, producing ROS (reactive oxygen species) to kill bacteria..

Magnesium Oxide (MgO): they increase oxidative stress and membrane disruption in bacteria.

3. Carbon-Based Antibacterial Materials

Graphene Oxide: They disrupt bacterial membranes and generates ROS.

Carbon Nanotubes: They physically puncture bacterial cell walls.

4. Ceramics and Clays

Zeolites: Zeolites embedded with silver or copper ions provide slow, sustained ion release.

Hydroxyapatite: They are often doped with metal ions like silver or zinc for antibacterial properties.

Polymer-based Antimicrobials: Certain polymers, either natural or synthetic, can possess inherent antibacterial properties or can be modified to incorporate antimicrobial agents. These materials have a wide range of uses, are long-lasting, and may be tailored to meet special requirements. By embedding antibacterial chemicals, functionalizing the polymer with active groups, or creating polymers that intrinsically contain antibacterial properties, it is possible

to create the antibacterial activity of these materials. Types of antibacterials polymers are listed below:

1. Polymers with Incorporated Antibacterial Agents

Polymers can be doped with silver, copper, or zinc nanoparticles. Similar to nanoparticles, polymers can also be incorporated with triclosan, chlorhexidine, or quaternary ammonium compounds.

2. Functionalized Polymers

Polymers functionalized with antibacterial chemical groups. Quaternary ammonium-functionalized polymers, for example, disrupt bacterial membranes via positively charged ammonium groups. Besides cationic polymers, phosphonium polymers can also kill bacteria by disrupting cell membranes. Polymeric brushes are another examples for antibacterial polymers. Polymers with surface-grafted chains functionalized with antibacterial moieties are very effective antibacterial materials..

3. Inherently Antibacterial Polymers

Chitosan is one of the most used one. It is a natural polymer derived from chitin with intrinsic antibacterial properties due to its cationic nature. Chitosan mimics the adhesive properties of mussels and can disrupt bacterial membranes.

Polyguanidines and Polybiguanides are the other example. Guanidine is a strong organic base. Thus the polymers of this type of material showed antibacterial activity. Poly(hexamethylene biguanide) (PHMB) is used in medical and textile applications.

4. Stimuli-Responsive Antibacterial Polymers

Polymers that become antibacterial under specific conditions (e.g., pH changes, temperature, or light) can be counted under this group. Photocatalytic polymers functionalized with titanium dioxide or antimicrobial peptides can be given as an example of this class of materials.

The selection of the appropriate antibacterial material depends on the specific application, the target bacterial strain, and the desired properties, such as antimicrobial efficacy, biocompatibility, and environmental impact.

The field of biobased antibacterial materials has garnered significant attention in recent years, as researchers and industry seek to develop more sustainable and environmentally friendly alternatives to traditional antimicrobial agents. Natural antimicrobials, such as essential oils, plant extracts, and antimicrobial peptides,

have shown promise in inhibiting bacterial growth and disrupting biofilm formation. For example, the essential oil of *Ocimum gratissimum* L. has been demonstrated to have potent antimicrobial effects against the spoilage bacterium *Shewanella putrefaciens*, highlighting the potential of natural compounds as effective antibacterial agents. (Xie et al., 2023). Bio-based antimicrobials, which are derived from or synthesized using biological sources, have also been extensively explored. These materials often exhibit reduced toxicity and environmental impact compared to synthetic antimicrobials, making them attractive alternatives. (Fan et al., 2018). Plant-derived natural products, such as flavonoids, terpenes, and phenolic compounds, have been investigated for their antibiofilm properties against problematic pathogens like *Pseudomonas aeruginosa* and *Staphylococcus aureus*. The mechanisms of action for these biobased antimicrobials can vary, including disruption of cell membranes, interference with cellular metabolism, and inhibition of quorum sensing pathways.

The development of biobased antibacterial materials requires a multidisciplinary approach, involving expertise from various fields, such as chemistry, materials science, microbiology, and engineering. Mainly used materials are petroleum based. Such as cetyltrimonium bromide are one of the best example of this type. Its chemical structure is cetyl trimethyl ammonium bromide. It is a cationic surface active agent. Instead of this compound, for example, biobased counterparts would be evaluated. Due to the sustainable development, many groups continue work on this subject.

The development of biobased antibacterial materials has gained significant momentum in recent years, driven by the need for more sustainable and eco-friendly alternatives to traditional antimicrobial agents. Natural antimicrobials, such as essential oils, plant extracts, and antimicrobial peptides, have shown promising results in inhibiting bacterial growth and disrupting biofilm formation (Fan et al., 2018; Beoletto et al., 2016). Biobased antimicrobials, which are derived from or synthesized using biological sources, have also been extensively explored. These materials often exhibit reduced toxicity and environmental impact compared to synthetic antimicrobials.

The specific action mechanisms of biobased antibacterial materials can vary, including disruption of cell membranes, interference with cellular metabolism,

and inhibition of quorum sensing pathways. The key resources needed for the research and development of biobased antibacterial materials include natural antimicrobial compounds, bioengineering and synthetic biology techniques, materials science and engineering expertise, testing and evaluation facilities, and resources for scaling and commercialization (Shamim et al., 2023; Fan et al., 2018; Xie et al., 2023; Guzzo et al., 2020).

CONCLUSION

The development of biobased antibacterial materials is a promising approach to address the growing concerns about antimicrobial resistance and environmental sustainability. Natural antimicrobials and biobased antimicrobials have demonstrated significant potential in inhibiting bacterial growth and disrupting biofilm formation. The key to the successful development of these materials lies in the continued research and collaboration across disciplines, leveraging the latest advancements in fields such as bioengineering, materials science, and microbiology. By addressing the technical, regulatory, and commercial challenges, biobased antibacterial materials can pave the way for a more sustainable and eco-friendly future in antimicrobial applications.

REFERENCES

- Agnihotri, S., & Dhiman, N. K. (2017). Development of Nano-Antimicrobial Biomaterials for Biomedical Applications. In *Advanced structured materials* (p. 479). Springer International Publishing. https://doi.org/10.1007/978-981-10-3328-5_12
- Aljaafari, M. N., AlAli, A. O., Baqais, L., Alqubaisy, M., AlAli, M., Molouki, A., Ong-Abdullah, J., Abushelaibi, A., Lai, K. -S., & Lim, S. -H. E. (2021). An Overview of the Potential Therapeutic Applications of Essential Oils. *Molecules*, 26(3), 628. <https://doi.org/10.3390/molecules26030628>
- Babu, R., O'Connor, K. E., & Ramakrishna, S. (2013). Current progress on bio-based polymers and their future trends. In *Progress in Biomaterials* (Vol. 2, Issue 1, p. 8). Springer Nature. <https://doi.org/10.1186/2194-0517-2-8>
- Beoletto, V. G., Oliva, M. de las M., Marioli, J. M., Carezzano, M. E., & Demo, M.

- S. (2016). Antimicrobial Natural Products Against Bacterial Biofilms. In Elsevier eBooks (p. 291). Elsevier BV. <https://doi.org/10.1016/b978-0-12-803642-6.00014-9>
- Fan, X., Ngo, H. L., & Wu, C. (2018). Natural and Bio-based Antimicrobials: A Review [Review of Natural and Bio-based Antimicrobials: A Review]. ACS Symposium Series, 1. American Chemical Society. <https://doi.org/10.1021/bk-2018-1287.ch001>
- Guzzo, F., Scognamiglio, M., Fiorentino, A., Buommino, E., & D'Abrosca, B. (2020). Plant Derived Natural Products against *Pseudomonas aeruginosa* and *Staphylococcus aureus*: Antibiofilm Activity and Molecular Mechanisms [Review of Plant Derived Natural Products against *Pseudomonas aeruginosa* and *Staphylococcus aureus*: Antibiofilm Activity and Molecular Mechanisms]. *Molecules*, 25(21), 5024. Multidisciplinary Digital Publishing Institute. <https://doi.org/10.3390/molecules25215024>
- Han, G., Guo, R., Yu, Z., & Chen, G. (2020). Progress on biodegradable films for antibacterial food packaging. In *E3S Web of Conferences* (Vol. 145, p. 1036). EDP Sciences. <https://doi.org/10.1051/e3sconf/202014501036>
- Khan, S. A., & Shakoor, A. (2023). Recent Strategies and Future Recommendations for the Fabrication of Antimicrobial, Antibiofilm, and Antibiofouling Biomaterials [Review of Recent Strategies and Future Recommendations for the Fabrication of Antimicrobial, Antibiofilm, and Antibiofouling Biomaterials]. *International Journal of Nanomedicine*, 3377. Dove Medical Press. <https://doi.org/10.2147/ijn.s406078>
- Kirthika, S.K., Goel, G., Matthews, A., Goel, S., (2023). Review of the untapped potentials of antimicrobial materials in the construction sector, *Progress in Materials Science*,133, 101065, <https://doi.org/10.1016/j.pmatsci.2022.101065>.
- Shamim, A., Ali, A., Iqbal, Z., Mirza, Mohd. A., Aqil, Mohd., Kawish, S. M., Siddiqui, A., Kumar, V., Naseef, P. P., Alshadidi, A. A. F., & Kuruniyan, M. S. (2023). Natural Medicine a Promising Candidate in Combating Microbial Biofilm [Review of Natural Medicine a Promising Candidate in Combating Microbial Biofilm]. *Antibiotics*, 12(2), 299. Multidisciplinary Digital Publishing Institute. <https://doi.org/10.3390/antibiotics12020299>
- Xie, Y., Zhang, C., Mei, J., & Xie, J. (2023). Antimicrobial Effect of *Ocimum gratissimum* L. Essential Oil on *Shewanella putrefaciens*: Insights Based

on the Cell Membrane and External Structure. In International Journal of Molecular Sciences (Vol. 24, Issue 13, p. 11066). Multidisciplinary Digital Publishing Institute. <https://doi.org/10.3390/ijms241311066>

CHAPTER 8

MOLECULAR DOCKING STUDIES OF CEPHALOSPORIN AND OXYTETRACYCLINE WITH ESCHERICHIA COLI DNA GYRASE

Assoc. Prof. Dr. Alev ER

Istanbul University

Science Faculty, Physics Department

ORCID NO: 0000-0002-3190-5342

Prof. Dr. Sefa CELIK

Istanbul University

Science Faculty, Physics Department

ORCID NO: 0000-0001-6216-1297

Prof. Dr. Aysen E. OZEL

Istanbul University

Science Faculty, Physics Department

ORCID NO: 0000-0002-8680-8830

Prof. Dr. Sevim AKYUZ

Istanbul Kultur University

Science Faculty, Physics Department

ORCID NO: 0000-0003-3313-6927

INTRODUCTION

Because of its rather nefarious connection with humans, *E. coli*'s prevalence in the environment is concerning. According to Russo and Johnson (2003) and Kaper et al. (2004), *E. coli* is a leading cause of diarrheal illnesses, peritonitis, colitis, bacteremia, newborn mortality, and urinary tract infections. These illnesses cost billions of dollars to treat globally and claim the lives of around 2 million people annually. According to Arthur et al. (2012), some strains may potentially cause cancer. When exposed to unwell hosts or to areas of a host's body other than the stomach, some opportunistic *E. coli* infections are brought on by strains of the bacteria that are typically benign or helpful (Kaper et al., 2004).

While the majority of *E. coli* strains are innocuous, some are pathogenic and can cause illnesses such as bloody or watery diarrhea, meningitis, sepsis, and tract infections, which can lead to death (Cho et al., 2018).

In 2011, 589,854 instances of waterborne diseases were recorded in 58 countries worldwide, according to the World Health Organization's (WHO) study titled "Water Quality and Health Strategy" for 2013-2020 (WHO, 2013). The Austrian physician Theodor von Escherich discovered *Escherichia coli* (*E. coli*), a member of the Enterobacteriaceae family and one of the harmful bacteria that may be found in water. *E. Coli* is one of the bacterial species that inhabit living things' big intestines. Nevertheless, it may live for 4–12 weeks, depending on the habitat, and pollutes spring waters by polluting them with the waste products of living things (Edberg et al., 2000; Değirmenci et al., 2019).

A broad class of similar β -lactam antibiotics are known as cephalosporins. The cephalosporins' low toxicity rates, comparatively wide range of action, and simplicity of administration are among their advantages. Pneumonia, bacteremia, meningitis, and infections of the skin and soft tissues can all be effectively treated with different cephalosporins. Although the many cephalosporin antimicrobial drugs can differ in small ways, knowing these variances is crucial for using them to their full potential (Marshall et al., 1999).

Beta-lactam antibiotics, such as cephalosporins, function similarly to penicillins and have a similar structure. The four-membered "core" beta-lactam ring of cephalosporins and penicillins is identical; however, cephalosporins have one

extra atom in the side ring. Either ring's side chains can change pharmacokinetics, beta-lactamase resistance, or antibacterial action. Most microorganisms that are sensitive to penicillins are also susceptible to cephalosporins. *Pasteurella sp.* and *Listeria* are exceptions. Although all methicillin-resistant *S aureus* (MRSA) and *enterococci* are cephalosporin-resistant, cephalosporins are effective against common gram-negative bacteria like *Escherichia coli*, nontypeable *Haemophilus influenzae* (ntHi), and methicillin-susceptible *Staphylococcus aureus* (MSSA) (Christopher et al., 2008).

Cephalosporins are the most significant family of antibiotics that target the penicillin binding protein (PBP), according to their structure activity relationship (SAR), chemical makeup, and other pharmacological characteristics. Among all the cephalosporins, cefixime is the preferred medication primarily because of its ability to withstand β -lactamase. However, compared to other antibiotics, this family of antibiotics has a greater level of coverage against gram-negative bacteria. The benefits of cephalosporins for patients in the healthcare system are increased by a thorough investigation of their pharmacological and chemical characteristics. Pharmacogenetics is a new field of study that focuses on how genetic and environmental variables might change a drug's pharmacology (Shahbaz, 2016; 2017).

Oxytetracycline is a naturally occurring broad-spectrum antibiotic that is widely used in aquaculture around the world because it inhibits the synthesis of proteins, which gives it broad-spectrum activity against both Gram-positive and Gram-negative bacteria and minimal host side effects (Yang et al., 2019; Chopra et al., 2001; Navarrete et al., 2008). Numerous bacterial diseases that pose serious challenges to the tilapia industry, such as Francisellosis, motile *Aeromonas* septicemia, and Streptococcosis, have been successfully treated with over-the-counter (OTC) treatments (Favero et al., 2021; Roy et al., 2019; Oviedo-Bolaños et al., 2021; Payne et al., 2021).

In this study to evaluate the binding mechanisms and interactions of cephalosporin and oxytetracycline with *Escherichia coli* DNA gyrase, molecular docking studies were performed and binding modes and binding energies of cephalosporin-6f86 and oxytetracycline-6f86 complexes were determined.

METHODS AND CALCULATIONS

The molecular structures of cephalosporin (PubChem CID 25058126) and oxytetracycline (PubChem CID 54675779) were obtained from the National Library of medicine, were subjected to energy minimization procedure using the YASARA program (Krieger et al., 2014) with the NOVA force field (Krieger et al., 2002). The energy-minimized oxytetracycline and cephalosporin molecules were then utilized as input for the docking simulation. Additionally, before the docking simulations, the receptors from the protein databank (PDB ID: 6f86) (Narramore et al., 2019) underwent the energy reduction procedure of the YASARA structure program utilizing the NOVA force field.

Molecular docking was studied using the YASARA program (v22.9.24) and the VINA docking technique (Trott et al., 2010). After removing the ligands and water molecules from the PDB data and adding polar hydrogen atoms, the downloaded target protein was ready for docking. The target's Kollman charges were calculated.

RESULTS

The binding energies of cephalosporin and oxytetracycline complexes docked with *Escherichia coli* DNA gyrase were found to be -6.691 kcal/mol and -6.938 kcal/mol, respectively. Three-dimensional docking models of the cephalosporin and oxytetracycline complexes in the *Escherichia coli* DNA gyrase active site are displayed in Figures 1 and 2.

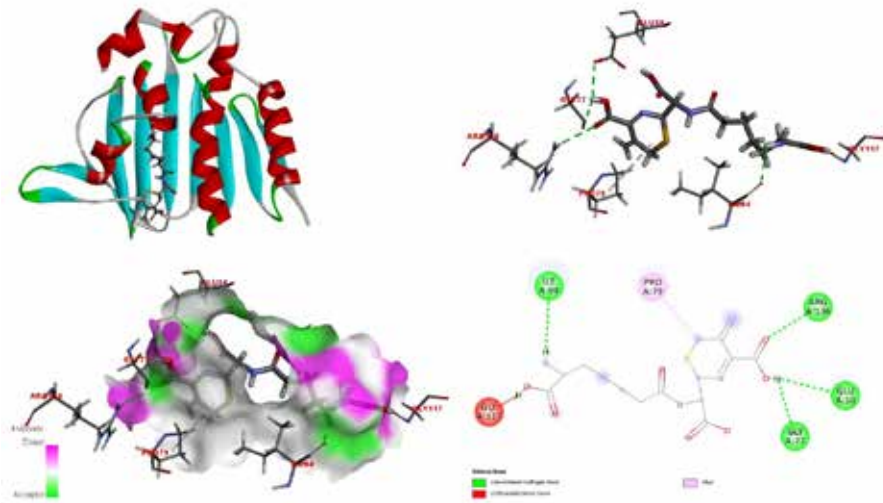


Figure 1. In the molecular docked model of Cephalosporin with Escherichia coli DNA gyrase (PDB ID: 6f86), the interactions between the Cephalosporin and Escherichia coli DNA gyrase are labeled using colored dashed lines (binding energy -6.691 kcal/mol).

The interactions determined by calculation between the Escherichia coli DNA gyrase (PDB ID: 6f86) and Cephalosporin are as follows;

- 2.87 Å long hydrogen bond with GLU50;
- 2.91 Å long hydrogen bond with GLY77;
- 4.62 Å long alkyl interaction with PRO79;
- 2.54 Å long hydrogen bond with ILE94;
- 0.99 Å long unfavorable donor-donor interaction with GLY117;
- 2.95 Å long hydrogen bond with ARG136.

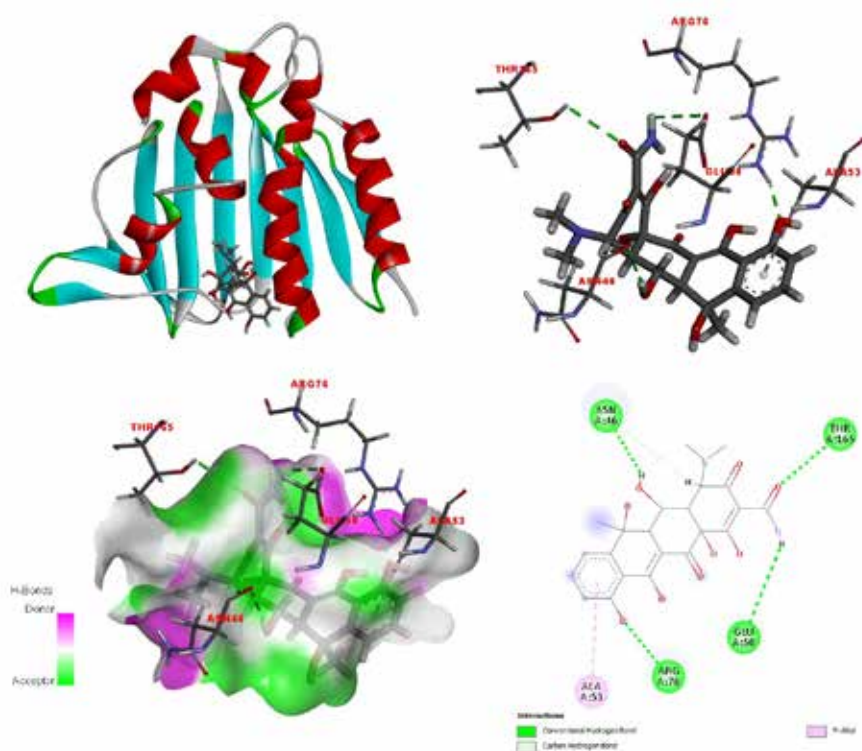


Figure 2. In the molecular docked model of Oxytetracycline with Escherichia coli DNA gyrase (PDB ID: 6f86), the interactions between the Oxytetracycline and Escherichia coli DNA gyrase are labeled using colored dashed lines (binding energy -6.938 kcal/mol).

The interactions determined by calculation between the Escherichia coli DNA gyrase (PDB ID: 6f86) and Oxytetracycline are as follows;

2.50 Å long hydrogen bond and 2.94 Å long carbon-hydrogen bond with ASN46;

3.06 Å long hydrogen bond with GLU50;

4.56 Å long pi-alkyl interaction with ALA53;

2.05 Å long hydrogen bond with ARG76;

3.04 Å long hydrogen bond with THR165.

CONCLUSIONS

Cephalosporin and Oxytetracycline complexes were shown to have high binding energies of -6.691 kcal/mol and -6.938 kcal/mol, respectively, based on the findings of molecular docking calculations of these drugs with *E. coli* DNA gyrase (PDB ID: 6f86). According to the results, these compounds are a good choice for treating *E. coli*.

REFERENCES

- Arthur, J. C., Perez-Chanona, E., Mühlbauer, M., Tomkovich, S., Uronis, J. M., Fan, T. J., ... & Jobin, C. (2012). Intestinal inflammation targets cancer-inducing activity of the microbiota. *science*, 338(6103), 120-123.
- Cho, S., Hiott, L. M., Barrett, J. B., McMillan, E. A., House, S. L., Humayoun, S. B., ... & Frye, J. G. (2018). Prevalence and characterization of *Escherichia coli* isolated from the Upper Oconee Watershed in Northeast Georgia. *PLoS One*, 13(5), e0197005.
- Chopra, I., & Roberts, M. (2001). Tetracycline antibiotics: mode of action, applications, molecular biology, and epidemiology of bacterial resistance. *Microbiology and molecular biology reviews*, 65(2), 232-260.
- Christopher, J., & Denis, B. (2008). Cephalosporins; A review. *Pediatrics in review*, 29(8), 264-73.
- Değirmenci, E., Kaloğlu, A. H., Güven, E., Durak, S., & Orbuk, H. (2019). İçme sularında bulunan *E. Coli* bakterilerinin görüntü işleme yöntemleriyle tespiti. *Çukurova Üniversitesi Mühendislik-Mimarlık Fakültesi Dergisi*, 34(3), 235-246.
- Edberg, S. C. L., Rice, E. W., Karlin, R. J., & Allen, M. J. (2000). *Escherichia coli*: the best biological drinking water indicator for public health protection. *Journal of applied microbiology*, 88(S1), 106S-116S.
- Favero, L. M., Facimoto, C. T., Chideroli, R. T., da Costa, A. R., Umezu, D. F., Honda, B. T. B., ... & Pereira, U. D. P. (2021). Administration of dehydrated oxytetracycline effectively reduces francisellosis mortality in Nile tilapia. *Aquaculture Research*, 52(9), 4116-4126.

- Kaper, J. B., Nataro, J. P., & Mobley, H. L. (2004). Pathogenic escherichia coli. *Nature reviews microbiology*, 2(2), 123-140.
- Krieger, E., Koraimann, G., Vriend, G. (2002) Increasing the precision of comparative models with YASARA NOVA-a self-parameterizing force field, *Proteins: Structure, Function, and Bioinformatics*, 47(3), 393-402.
- Krieger, E., Vriend, G. (2014) YASARA View-molecular graphics for all devices—from smartphones to workstations, *Bioinformatics*, 30(20), 2981-2982.
- Marshall, W. F., & Blair, J. E. (1999, February). The cephalosporins. In *Mayo Clinic Proceedings* (Vol. 74, No. 2, pp. 187-195). Elsevier.
- Narramore, S., Stevenson, C. E., Maxwell, A., Lawson, D. M., & Fishwick, C. W. (2019). New insights into the binding mode of pyridine-3-carboxamide inhibitors of E. coli DNA gyrase. *Bioorganic & medicinal chemistry*, 27(16), 3546-3550.
- Navarrete, P., Mardones, P., Opazo, R., Espejo, R., & Romero, J. (2008). Oxytetracycline treatment reduces bacterial diversity of intestinal microbiota of Atlantic salmon. *Journal of Aquatic Animal Health*, 20(3), 177-183.
- Oviedo-Bolaños, K., Rodríguez-Rodríguez, J. A., Sancho-Blanco, C., Barquero-Chanto, J. E., Peña-Navarro, N., Escobedo-Bonilla, C. M., & Umaña-Castro, R. (2021). Molecular identification of Streptococcus sp. and antibiotic resistance genes present in Tilapia farms (*Oreochromis niloticus*) from the Northern Pacific region, Costa Rica. *Aquaculture International*, 29(5), 2337-2355.
- Payne, C. J., Turnbull, J. F., MacKenzie, S., & Crumlish, M. (2021). Investigating the effect of an oxytetracycline treatment on the gut microbiome and antimicrobial resistance gene dynamics in Nile Tilapia (*Oreochromis niloticus*). *Antibiotics*, 10(10), 1213.
- Roy, A., Abraham, T. J., Namdeo, M. S., Singha, J., Julinta, R. B., & Boda, S. (2019). Effects of oral oxytetracycline-therapy on wound progression and healing following *Aeromonas caviae* infection in Nile tilapia (*Oreochromis niloticus* L.). *Brazilian Archives of Biology and Technology*, 62, e19180766.
- Russo, T. A., & Johnson, J. R. (2003). Medical and economic impact of extraintestinal infections due to *Escherichia coli*: focus on an increasingly important endemic problem. *Microbes and infection*, 5(5), 449-456.
- Shahbaz, K. (2016). Pharmenzymonetics And Pharmgeonetics: A New Door In Pharmacology. *World Journal of Pharmacy and Pharmaceutical Sciences*.

- Shahbaz, K. (2017). Cephalosporins: pharmacology and chemistry. *Pharmaceutical and Biological Evaluations*.
- Trott, O., Olson, A. J. (2010) AutoDock Vina: improving the speed and accuracy of docking with a new scoring function, efficient optimization, and multithreading, *Journal of computational chemistry*, 31(2), 455-461.
- WHO, 2013, Water Quality and Health Strategy 2013-2020.
- Yang, T., Yang, K., Chen, Y., & Fan, K. (2019). Characterization of a Bi-directional promoter OtrRp involved in oxytetracycline biosynthesis. *Current Microbiology*, 76, 1264-1269.